PHYSICAL REVIEW D **82,** 114506 (2010)

$D \to K, l\nu$ semileptonic decay scalar form factor and $|V_{cs}|$ from lattice QCD

Heechang Na,[1] Christine T. H. Davies,[2] Eduardo Follana,[3] G. Peter Lepage,[4] and Junko Shigemitsu[1]

(HPQCD Collaboration)

[1]*Department of Physics, The Ohio State University, Columbus, Ohio 43210, USA*
[2]*Department of Physics and Astronomy, University of Glasgow, Glasgow, G12 8QQ, United Kingdom*
[3]*Departmento de Fisica Teorica, Universidad de Zaragoza, Zaragoza, Spain*
[4]*Laboratory of Elementary Particle Physics, Cornell University, Ithaca, New York 14853, USA*
(Received 30 August 2010; published 9 December 2010)

We present a new study of D semileptonic decays on the lattice which employs the highly improved staggered quark action for both the charm and the light valence quarks. We work with MILC unquenched $N_f = 2 + 1$ lattices and determine the scalar form factor $f_0(q^2)$ for $D \to K, l\nu$ semileptonic decays. The form factor is obtained from a scalar current matrix element that does not require any operator matching. We develop a new approach to carrying out chiral/continuum extrapolations of $f_0(q^2)$. The method uses the kinematic "z"variable instead of q^2 or the kaon energy E_K and is applicable over the entire physical q^2 range. We find $f_0^{D\to K}(0) \equiv f_+^{D\to K}(0) = 0.747(19)$ in the chiral plus continuum limit and hereby improve the theory error on this quantity by a factor of ~4 compared to previous lattice determinations. Combining the new theory result with recent experimental measurements of the product $f_+^{D\to K}(0) * |V_{cs}|$ from *BABAR* and CLEO-c leads to a very precise direct determination of the CKM matrix element $|V_{cs}|$, $|V_{cs}| = 0.961(11)(24)$, where the first error comes from experiment and the second is the lattice QCD theory error. We calculate the ratio $f_+^{D\to K}(0)/f_{D_s}$ and find 2.986 ± 0.087 GeV^{-1} and show that this agrees with experiment.

DOI: 10.1103/PhysRevD.82.114506 PACS numbers: 12.38.Gc, 13.20.Fc, 13.20.He

I. INTRODUCTION

Independent determinations of each of the Cabibbo-Kobayashi-Maskawa (CKM) matrix elements and checks of three generation unitarity provide stringent consistency tests of the standard model and have become an important part of flavor physics. For instance, first row unitarity has now been checked to very high accuracy with $|V_{ud}|^2 + |V_{us}|^2 + |V_{ub}|^2 - 1 = -0.0001(6)$ [1]. Such precision became possible when both experiment and lattice QCD theory inputs to the determination of $|V_{us}|$ reached subpercent levels of accuracy (the contribution from $|V_{ub}|$ to the unitarity sum is negligible and $|V_{ud}|$ is known with ~0.02% errors).

In contrast to the elements of the 1st row, direct determinations of the 2nd row matrix elements are still much less precise. The latest PDG summary [2] quotes 4.8%, 3.5%, and 3.2% errors for $|V_{cd}|$, $|V_{cs}|$, and $|V_{cb}|$, respectively when one considers all ways of extracting the matrix elements. If one focuses just on determinations of $|V_{cd}|$ and $|V_{cs}|$ from semileptonic $D \to \pi, l\nu$ and $D \to K, l\nu$ decays, until recently the total error has been at the 10% level and dominated by lattice QCD theory errors. Furthermore, tests of 2nd row unitarity stands at $|V_{cd}|^2 + |V_{cs}|^2 + |V_{cb}|^2 = 1.101 \pm 0.074$ and for the 2nd column at $|V_{us}|^2 + |V_{cs}|^2 + |V_{ts}|^2 = 1.099 \pm 0.074$ [2]. In both cases the error is dominated by the uncertainty in $|V_{cs}|$. Clearly reducing the errors in $|V_{cs}|$ will have an immediate and significant impact on flavor physics and on CKM unitarity tests. On the experimental front Belle [3], *BABAR* [4], and CLEO-c [5] have all recently published precise measurements of the combination $f_+^{D\to K}(0) * |V_{cs}|$ with 3.3%, 1.4%, and 1.1% errors, respectively. These precise measurements can be turned into accurate $|V_{cs}|$ determinations if and only if theory can provide the form factor $f_+^{D\to K}(0)$ with comparable precision. The main goal of the current work was to improve lattice QCD calculations of $f_+^{D\to K}(0)$ and the outcome is that we have now succeeded in reducing the theory errors from 10% down to 2.5%. Innovations that made this dramatic improvement in errors possible include the employment of a new and better action for charm quarks, the use of an absolutely normalized hadronic matrix element that does not require any operator matching, improved analysis tools for lattice data, and a new method for carrying out chiral/continuum extrapolations.

One reason for the large disparity in the size of lattice QCD errors between kaon and D meson systems in the past has been the challenge of simulating quarks with masses as large as that of the charm quark. If "a"is the lattice spacing and hence $\sim 1/a$ the cutoff in the theory, then for charm quarks it was thought to be difficult to satisfy $am_c = m_c/\text{cutoff} \ll 1$. In the past this problem was circumvented by employing effective theories to handle the charm quark, nonrelativistic QCD, HQET, or the "heavy clover" action of the Fermilab lattice collaboration. The first $N_f = 2 + 1$ unquenched studies of D semileptonic decays on the lattice

were carried out by the Fermilab Lattice and MILC collaborations using an effective theory for charm [6]. This pioneering work predicted the shape of the form factors as a function of q^2 prior to subsequent verification by experiment. The theory errors, however, were quite large at $\sim$10%. The calculations by the Fermilab Lattice and MILC collaborations are being improved upon and their theory errors should be reduced significantly soon [7]. On the other hand, working with effective theories typically leads to larger statistical and systematic errors than when employing ''relativistic'' quark actions as can be done for kaon physics. This includes uncertainties coming from matching of heavy-light currents responsible for heavy meson leptonic or semileptonic decays, and from the tuning of heavy quark masses, all procedures that are much more complicated in effective theories.

In recent years there has been a major shift in lattice simulations with charm quarks. With the advent of highly improved lattice quark actions, the concerns described above of m_c/cutoff being too large have been overcome and several collaborations are now working on charm physics without resorting to effective theories. In 2007 the HPQCD collaboration introduced the ''highly improved staggered quark'' (HISQ) action [8]. Many lattice artifacts, including all $\mathcal{O}((am_c)^2)$ discretization effects and all $\mathcal{O}(\alpha_s(am_c)^2)$ and $\mathcal{O}((am_c)^4)$ effects at leading order in the charm quark velocity $\frac{v}{c}$ have been removed. It then becomes feasible to simulate charm quarks on the lattice in a fully relativistic setting without introducing large discretization errors as long as one works with lattice spacings $a \leq \sim 0.15$ fm. This last condition is easily met nowadays in typical lattice simulations. Another approach to charmed meson leptonic and semileptonic decays using relativistic charm quarks is being pursued by the European Twisted Mass (ETM) collaboration [9]. They employ a special version of Wilson type quark action called the ''twisted mass'' quark action where discretization errors come in at $\mathcal{O}(a^2)$.

The HPQCD collaboration has successfully applied HISQ charm quarks to studies of D and D_s meson leptonic decays [10]. This formalism significantly reduced lattice errors in decay constant calculations. We have now also initiated D meson semileptonic decay studies based on HISQ charm and light valence quarks. In Ref. [11] we developed and tested our approach on a simpler test case of a fictitious $D_s \to \eta_s, l\nu$ semileptonic decay (η_s refers to a pseudoscalar $s - \bar{s}$ bound state). In the current paper we present the first application of HISQ charm quarks to realistic D meson semileptonic decays. More specifically, we calculate the scalar form factor $f_0(q^2)$ for $D \to K, l\nu$ decays. As mentioned above already experiment provides us with the product $f_+(0) * |V_{cs}|$. Then using the kinematic relation $f_0(0) = f_+(0)$, an accurate calculation of $f_0(q^2)$ from the lattice leads to a precise determination of the CKM matrix element $|V_{cs}|$.

We have carried out simulations on three of the MILC ''coarse'' ensembles with lattice spacing $a \sim 0.12$ fm and two of the ''fine'' ensembles with $a \sim 0.09$ fm. Details of these ensembles are listed in Table I. The five ensembles provide enough variation and information to allow sensible chiral and continuum extrapolations to the physical world.

In the next section we review the formalism for extracting semileptonic decay form factors from hadronic matrix elements of appropriate heavy-light currents. We describe the advantages of working with the same relativistic action for both the heavy and the light quarks and explain why the form factor at $q^2 = 0$ is most accurately extracted from hadronic matrix elements of the scalar current as opposed to from the vector current. In Sec. III we introduce the HISQ action and describe how action parameters such as bare quark masses were tuned. Section IV provides further details of our simulations including benefits derived from using ''random wall'' sources, in particular, when simulating kaons with nonzero momenta. Section V describes our fitting strategy. We have invested considerable effort into developing improved fitting methods in order to extract the form factors of interest with subpercent errors for each ensemble and for all kaon momenta needed to cover the physical q^2 range.

In Sec. VI we take the form factor results from the five ensembles and extrapolate to the chiral/continuum limit. To this end we have developed a new extrapolation method that can be used over the entire physical q^2 range, $(M_D - M_K)^2 \geq q^2 \geq 0$. Since we are interested in the form factor at $q^2 = 0$, it is important that any extrapolation scheme work all the way down to $q^2 = 0$ where the kaon in the D

TABLE I. Details of MILC configurations employed in this article. N_{tsrc} is the number of time sources used per configuration. All sea quark masses are given in the MILC collaboration normalization convention with $u_0^{\text{plaq}} = \langle \text{plaquette} \rangle^{1/4}$. Values for the scale variable r_1 in lattice units, r_1/a, are taken from Ref. [12]. Errors in this ratio are at the $\sim$0.1% level.

Set	r_1/a	au_0m_{sea}	u_0^{plaq}	N_{conf}	N_{tsrc}	$L^3 \times N_t$
C1	2.647	0.005/0.050	0.8678	600	2	$24^3 \times 64$
C2	2.618	0.010/0.050	0.8677	600	2	$20^3 \times 64$
C3	2.644	0.020/0.050	0.8688	600	2	$20^3 \times 64$
F1	3.699	0.0062/0.031	0.8782	600	4	$28^3 \times 96$
F2	3.712	0.0124/0.031	0.8788	600	4	$28^3 \times 96$

meson rest frame has energy $E_K \approx 1$ GeV. The new approach uses the "z expansion" of Refs. [13–15] to parametrize the kinematics (the dependence on E_k or equivalently on q^2). The coefficients of this expansion are then allowed to be functions of the light and strange quark masses and of the lattice spacing. We find that good fits to all our data are possible with such an ansatz and the resulting $f_0(0)$ in the chiral/continuum limit is very stable against higher order terms in this ansatz.

Section VII summarizes our final results for $f_0(0) = f_+(0)$ at the physical point and explains our error budget. We incorporate experimental input from *BABAR* [4] and CLEO-c [5] to determine the CKM matrix element $|V_{cs}|$ and compare with values listed in the PDG and with expectations from CKM unitarity. In Sec. VIII we collect results obtained as "side products" of our analysis of semileptonic decay three-point hadronic matrix elements, namely, results coming from two-point correlators such as decay constants of the pion, kaon, D and D_s mesons. These two-point results provide nontrivial tests of our mass tunings, fitting, and chiral/continuum extrapolation strategies leading to greater confidence in our form factor (i.e. three-point) results as well. Finally, Sec. IX gives a summary and addresses future plans. Several appendices cover details of Bayesian fits employed in this article. In Appendix C we carry out the chiral/continuum extrapolation of $f_0(q^2)$ using an approach that differs completely from the z-expansion method of Sec. VI and is based instead on chiral perturbation theory. We show that the two extrapolation methods give results in very good agreement with each other.

II. FORMALISM

To study the process $D \to K, l\nu$ one needs to evaluate the matrix element of the charged electroweak current between the D and the K meson states, $\langle K|(V^\mu - A^\mu)|D\rangle$. Only the vector current V^μ contributes to the pseudoscalar-to-pseudoscalar amplitude and the matrix element can be written in terms of two form factors $f_+(q^2)$ and $f_0(q^2)$, where $q^\mu = p_D^\mu - p_K^\mu$ is the four-momentum of the emitted W boson:

$$\langle K|V^\mu|D\rangle = f_+^{D\to K}(q^2)\left[p_D^\mu + p_K^\mu - \frac{M_D^2 - M_K^2}{q^2}q^\mu\right] + f_0^{D\to K}(q^2)\frac{M_D^2 - M_K^2}{q^2}q^\mu \quad (1)$$

with $V^\mu \equiv \bar{\Psi}_s\gamma^\mu\Psi_c$. As described below, we find it useful to consider also the matrix element of the scalar current $S \equiv \bar{\Psi}_s\Psi_c$,

$$\langle K|S|D\rangle = \frac{M_D^2 - M_K^2}{m_{0c} - m_{0s}}f_0^{D\to K}(q^2). \quad (2)$$

In continuum QCD one has the partially conserved vector current (PCVC) relation and the vector and scalar currents obey

$$q^\mu\langle V_\mu^{\rm cont}\rangle = (m_{0c} - m_{0s})\langle S^{\rm cont}\rangle. \quad (3)$$

In fact, PCVC is the reason why the same form factor $f_0^{D\to K}(q^2)$ appears in Eqs. (1) and (2). On the lattice, it is often much more convenient to simulate with vector currents $\bar{\Psi}_{Q1}\gamma^\mu\Psi_{Q2}$ that are not exactly conserved at finite lattice spacings even for $Q1 = Q2$. Such non-exactly-conserved currents need to be renormalized and acquire Z factors. We are able to carry out fully nonperturbative renormalization of the lattice vector current by imposing PCVC. In the D meson rest frame the condition becomes

$$(M_D - E_K)\langle V_0^{\rm latt}\rangle Z_t + \vec{p}_K\cdot\langle\vec{V}^{\rm latt}\rangle Z_s = (m_{0c} - m_{0s})\langle S^{\rm latt}\rangle. \quad (4)$$

We have checked the feasibility of this renormalization scheme and extracted preliminary Z_t and Z_s values for the test case of $D_s \to \eta_s, l\nu$ mentioned above in Ref. [11]. We plan to apply this fully nonperturbative renormalization scheme to evaluate $\langle\pi|V^\mu|D\rangle$ and $\langle K|V^\mu|D\rangle$ relevant for realistic $D \to \pi, l\nu$ and $D \to K, l\nu$ semileptonic decays in the near future. In the present article, however, we will focus on the form factor $f_+(q^2)$ just at $q^2 = 0$, since this is all that is needed to extract $|V_{cs}|$. We do this by exploiting the kinematic identity $f_+(0) = f_0(0)$, and concentrating on determining the scalar form factor $f_0(q^2)$ as accurately as possible. The best way to proceed is to evaluate the hadronic matrix element of the scalar current rather than of the vector current. From Eq. (2), one then has

$$f_0^{D\to K}(q^2) = \frac{(m_{0c} - m_{0s})\langle K|S|D\rangle}{M_D^2 - M_K^2}. \quad (5)$$

The numerator on the right-hand side is a renormalization group invariant combination. This is true even in our lattice formulation, because we use the same relativistic action for both the heavy and the light valence quarks. Moreover, Eq. (5) allows a lattice determination of $f_0(q^2)$ and hence also of $f_+(0) = f_0(0)$ without any need for operator matching. Using Eq. (5) and going to the continuum limit is straightforward, because our action is so highly improved even for heavy quarks.

III. THE HISQ ACTION AND TUNING OF ACTION PARAMETERS

The HISQ action was introduced in Ref. [8] and represents the next level of improvement of staggered quarks beyond the AsqTad [16] action. Relative to the latter, the HISQ action reduces taste breaking effects by approximately a factor of 3 on MILC coarse and fine lattices. For heavy quarks such as charm the HISQ action includes one adjustable parameter ϵ which modifies the "Naik" term already present in the AsqTad action $\frac{1}{6}a^2\Delta_\mu^3 \to \frac{1+\epsilon}{6}a^2\Delta_\mu^3$. In Ref. [8] ϵ was adjusted nonperturbatively to get the correct dispersion relation for the η_c meson. It was found that one ends up with ϵ's close to estimates coming from requiring that the tree-level quark propagator have

TABLE II. Action parameters and η_c and η_s masses. $1+\epsilon$ enters the coefficient of the Naik term for charm propagators.

Set	am_{0c}	am_{0s}	am_{0l}	$1+\epsilon$	aM_{η_c}	aM_{η_s}
C1	0.6207	0.0489	0.0070	0.780	1.7887(1)	0.4111(2)
C2	0.6300	0.0492	0.0123	0.774	1.8085(1)	0.4143(2)
C3	0.6235	0.0491	0.0246	0.778	1.7907(1)	0.4118(2)
F1	0.4130	0.0337	0.00674	0.893	1.2807(1)	0.2942(1)
F2	0.4120	0.0336	0.01350	0.894	1.2751(1)	0.2931(2)

speed of light $c(p)=1$. In the current simulations we have set ϵ in the charm propagators equal to its tree-level value. The size of ϵ decreases rapidly with decreasing am_q, so for strange and light quarks ϵ can safely be set equal to zero. Table II lists the bare valence masses and the ϵ(charm) values employed for the five ensembles. The bare charm and strange quark masses were tuned in order to obtain the correct η_c and η_s meson masses. am_{0l} was chosen so that the ratio of HISQ valence masses m_{0l}(valence)$/m_{0s}$(valence) ended up close to the analogous ratio of light and "physical" strange quark masses for AsqTad quarks on the same ensemble.[1] This makes the valence light quark mass approximately equal to the sea light quark mass, both measured relative to a physical, tuned strange quark mass. Figures 1 and 2 show our results for the η_c and η_s masses on the five ensembles together with the target values. One sees that tuning has been achieved very accurately. For η_c our target value is $M_{\eta_c}^{\text{target}}=2.9852(34)$ GeV which differs slightly from the experimental $M_{\eta_c}^{\text{exper}}=2.9803$ GeV since we adjust for the absence of electromagnetic and annihilation effects in the lattice simulations [17]. The target value for the η_s is $M_{\eta_s}=0.6858(40)$ GeV [17]. The data points in Figs. 1 and 2 show only statistical and r_1/a errors. We first determine $r_1\times M_{\text{meson}}$ using the precisely know r_1/a for each ensemble. At this point, our data points have errors coming from both statistics and from the $\sim 0.1\%$ uncertainty in r_1/a (with the latter dominating). For the purposes of using a physical scale on the vertical axis, we then convert $r_1\times M_{\text{meson}}$ to MeV using $r1=0.3133(23)$ fm ($r_1^{-1}=0.6297(46)$ GeV) [17]. For reasons explained below, we find it more informative not to include the $\sim 0.7\%$ uncertainty in the physical value of r_1 in these plots. Including this error will affect all five data points in the same way without changing relative uncertainties.

Once the bare charm and strange quark masses have been fixed for each ensemble there are no adjustable parameters left when one goes on to determining other meson masses such as M_D or M_{D_s}, decay constants f_D, f_{D_s}, f_K, etc. or semileptonic form factors. In Fig. 3 we show results for M_D and M_{D_s}. Again the errors on the data points reflect statistical and r_1/a errors only. Any changes in the physical value of r_1 will shift all five data points uniformly without affecting their relative positions. Furthermore, chiral/continuum extrapolations would be carried out on $r_1\times M_{\text{meson}}$ with r_1 and its error coming in only after having extracted the physical limit. By omitting the full r_1 errors in Fig. 3, one can more easily identify discretization effects and light quark mass dependence. For instance, for M_{D_s} the difference between the coarse and fine ensemble results is at the ~ 6 MeV level or $\sim 0.3\%$ and the sea light quark mass dependence is essentially nonexistent. The 0.3% discretization effect should be compared to the $\sim 0.7\%$ uncertainty in r_1. One lesson to be learnt from this is the importance of tuning quark masses accurately enough so that results on the different ensembles agree to within the smaller r_1/a errors and not just to within the larger r_1 error. Otherwise it would not be possible to have data points lying along smooth curves as in Fig. 3 where discretization and light quark mass dependence can be clearly identified and distinguished from mass tuning and r_1 errors. Based on Figs. 1–3, we believe the HISQ action parameters have been fixed accurately enough in

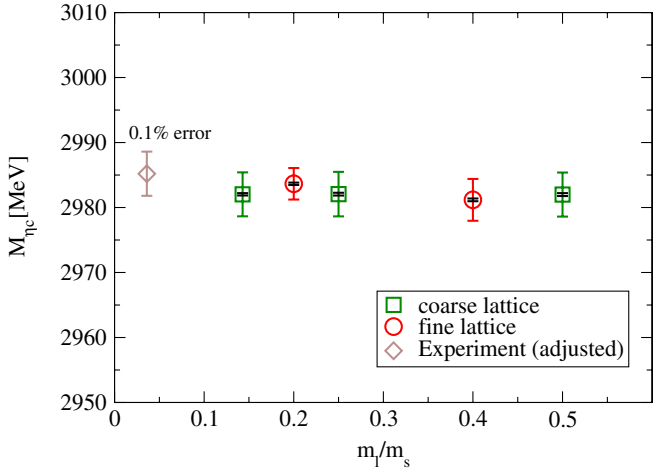

FIG. 1 (color online). Tuning of the charm quark mass via the η_c meson mass. Errors on the simulation results include statistical plus the $\sim 0.1\%$ errors coming from r_1/a. The smaller black error bars on the lattice data indicate the statistical errors. The "experimental" η_c mass has been adjusted to take into account the lack of annihilation and electromagnetic effects in our lattice calculation.

[1]Note that HISQ and AsqTad masses are not numerically the same, since the two actions are different.

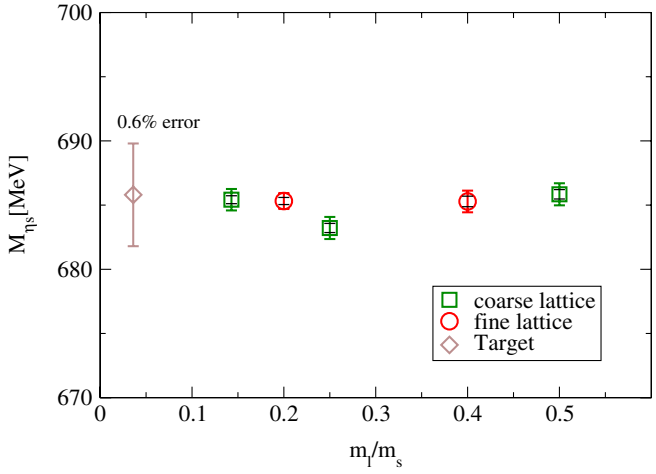

FIG. 2 (color online). Tuning of the strange quark mass via the η_s.

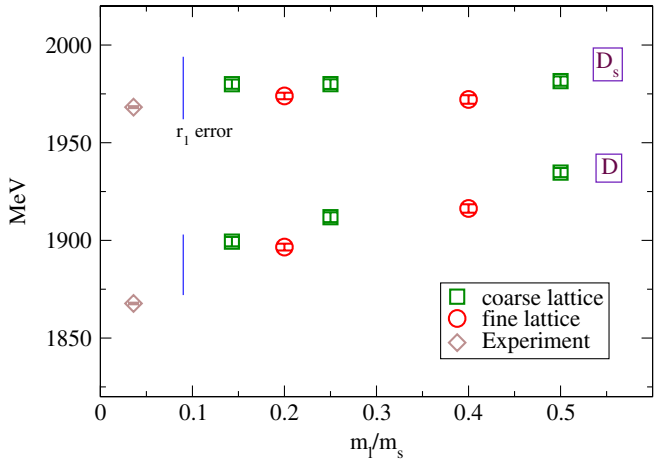

FIG. 3 (color online). The D and D_s meson masses. As explained in the text although the vertical axis uses physical units, the data points show statistical and r_1/a errors only. The experimental points have not been adjusted for electromagnetic effects that are absent in the lattice simulations. Such effects have been estimated to be less than 0.2% [21].

preparation for going on to D semileptonic decays. Further consistency checks, such as determinations of decay constants, will be given in Sec. VIII.

IV. SIMULATION DETAILS

The goal is to determine the hadronic matrix element $\langle K|S|D\rangle$ in Eq. (5) via numerical simulations. The starting point is the three-point correlator,

$$C^{3\,\mathrm{pnt}}(t_0, t, T, \vec{p}_K) = \frac{1}{L^3}\sum_{\vec{x}}\sum_{\vec{y}}\sum_{\vec{z}} e^{i\vec{p}_K\cdot(\vec{z}-\vec{x})}\langle\Phi_K(\vec{x}, t_0) \times \tilde{S}(\vec{z}, t)\Phi_D^\dagger(\vec{y}, t_0 - T)\rangle. \quad (6)$$

$\Phi_D^\dagger$ and Φ_K are interpolating operators that create a D meson or annihilate a kaon, respectively, and $\tilde{S} \equiv a^3 S$ is the scalar current in lattice units. We also work with dimensionless fermion fields. Equation (6) corresponds to first creating a zero momentum D meson at time $t_0 - T$ which propagates to time slice t with $t_0 \geq t \geq t_0 - T$. At time slice t, the scalar current $\tilde{S} = \bar{\Psi}_s\Psi_c$ converts the charm quark inside the D meson into a strange quark while inserting momentum $\vec{p}_K$. The resulting kaon is then annihilated at time t_0.

In our simulations we have picked t_0 the location of the kaon operator Φ_K randomly and differently for each configuration in order to reduce autocorrelations. We also worked with N_{tsrc} values of t_0 per configuration (see Table I) placed N_t/N_{tsrc} time slices apart (N_t is the total number of time slices for our lattices). Once t_0 was fixed, for each configuration we obtained results for several T values, $T = 15$ and 16 on coarse and $T = 19$, 20, and 23 on fine lattices. We will see later that having data at many T values significantly reduces errors in extracted three-point amplitudes. To further improve statistics, for each t_0 and T value we also evaluated the time-reversed three-point correlator, essentially the same as Eq. (6) but with $\Phi_D^\dagger$ acting on time slice $t_0 + T$ and the scalar current inserted at $T + t_0 \geq t \geq t_0$.

As is well known, with the HISQ action, each flavor of quark comes in N_{taste} copies called "tastes". One has $N_{\mathrm{taste}} = 4$ when working with one-component staggered fields and $N_{\mathrm{taste}} = 16$ for four-component "naive" fields. In the naive fields language the interpolating operators $\Phi_{D/K}$ and the scalar current $\tilde{S}$ become

$$\Phi_D^\dagger = \tfrac{1}{4}\bar{\Psi}_c\gamma_5\Psi_l, \qquad \Phi_K = \tfrac{1}{4}\bar{\Psi}_l\gamma_5\Psi_s, \quad (7)$$

and

$$\tilde{S} = \bar{\Psi}_s\Psi_c. \quad (8)$$

These are all single site bilinears. $\Phi_{D/K}$ correspond to taste nonsinglet "Goldstone" pseudoscalars and the factors of $\frac{1}{4} = \frac{1}{\sqrt{N_{\mathrm{taste}}}}$ serve to divide out traces over taste space. The scalar current in Eq. (8) is a taste singlet current. Carrying out the contractions over fermionic fields in $C^{3\,\mathrm{pnt}}$ and using the well-known relation between naive quark propagators $G_\Psi(x, y)$ and one-component field propagators $G_\chi(x, y)$,

$$G_\Psi(x, y) = \Omega(x)\Omega^\dagger(y)G_\chi(x, y) \quad (9)$$

with

$$\Omega(x) = \prod_{\mu=0}^{3}(\gamma_\mu)^{x_\mu}, \quad (10)$$

one obtains

$$\langle \Phi_K(x)\tilde{S}(z)\Phi_D^\dagger(y)\rangle = \frac{1}{16}\,\mathrm{Tr}\{G_{\Psi,s}(x,z)G_{\Psi,c}(z,y)\gamma_5 G_{\Psi,l}(y,x)\gamma_5\}$$
$$= \frac{1}{16}\,\mathrm{Tr}\{[\Omega(x)\Omega^\dagger(z)\Omega(z)\Omega^\dagger(y)\gamma_5\Omega(y)\Omega^\dagger(x)\gamma_5]G_{\chi,s}(x,z)G_{\chi,c}(z,y)G_{\chi,l}(y,x)\}$$
$$= \frac{1}{4}\,\phi(y)\phi(x)\,\mathrm{tr}\{G_{\chi,s}(x,z)G_{\chi,c}(z,y)G_{\chi,l}(y,x)\}$$
$$= \frac{1}{4}\,\phi(y)\phi(z)\,\mathrm{tr}\{G^\dagger_{\chi,s}(z,x)G_{\chi,c}(z,y)G_{\chi,l}(y,x)\}. \tag{11}$$

$\phi(y)$ stands for $(-1)^{\sum_\mu y_\mu}$ and similarly for $\phi(x)$ and $\phi(z)$. In the last step we have used $G_\chi(x,y) = \phi(x) * \phi(y)G^\dagger_\chi(y,x)$. "Tr" is the trace over spin and color and "tr" is the trace only over color. The three-point correlator can now be written as

$$C^{3\,\mathrm{pnt}}(t_0,t,T,\vec{p}_K) = \frac{1}{L^3}\sum_{\vec{x}}\sum_{\vec{y}}\sum_{\vec{z}} e^{i\vec{p}_K\cdot(\vec{z}-\vec{x})}\frac{1}{4}\phi(y)\phi(z)$$
$$\times\langle\,\mathrm{tr}\{G^\dagger_{\chi,s}(z,x)G_{\chi,c}(z,y)G_{\chi,l}(y,x)\}\rangle, \tag{12}$$

with $x_0 \equiv t_0$, $y_0 \equiv t_0 - T$, and $z_0 \equiv t$ and where $\langle\rangle$ now stands for average over configurations. One sees from Eq. (12) that strange HISQ propagators are needed going from $(\vec{x},t_0)$ to general z and light propagators again from $(\vec{x},t_0)$ to general y. If one actually wanted to carry out the $\frac{1}{L^3}\sum_{\vec{x}}$, one would need a strange and a light propagator from each spatial point on time slice t_0 and that would be prohibitively expensive. A common approach is to give up on doing the $\sum_{\vec{x}}$ and to use "local sources" where $\vec{x}$ is fixed at some $\vec{x}_0$, e.g. $\vec{x} = \vec{0}$. One then has

$$C^{3\,\mathrm{pnt}}_{loc}(t_0,t,T,\vec{p}_K) = \sum_{\vec{y}}\sum_{\vec{z}} e^{i\vec{p}_K\cdot\vec{z}}\times\frac{1}{4}\phi(y)\phi(z)$$
$$\times\langle\mathrm{tr}\{G^\dagger_{\chi,s}(z,x_{loc})G_{\chi,c}(z,y)$$
$$\times G_{\chi,l}(y,x_{\mathrm{loc}})\}\rangle, \tag{13}$$

with $x_{\mathrm{loc}} = (\vec{0},t_0)$. Momentum conservation will ensure that only kaons with momentum $\vec{p}_K$ contribute and be picked out at time slice t_0. On the other hand random wall sources allow us to carry out the $\frac{1}{L^3}\sum_{\vec{x}}$ without having to invert at each spatial point. This can be seen by writing

$$C^{3\,\mathrm{pnt}}_{rw}(t_0,t,T,\vec{p}_K) = \frac{1}{L^3}\sum_{\vec{x}}\sum_{\vec{x}'}\sum_{\vec{y}}\sum_{\vec{z}} e^{i\vec{p}_K\cdot(\vec{z}-\vec{x})}$$
$$\times\frac{1}{4}\phi(y)\phi(z)\langle\mathrm{tr}\{G^\dagger_{\chi,s}(z,x)G_{\chi,c}(z,y)$$
$$\times G_{\chi,l}(y,x')\times\xi^*(\vec{x})\xi(\vec{x}')\}\rangle. \tag{14}$$

$\xi(\vec{x})$ is a field of random U(1) phases, and $\langle\xi^*(\vec{x})\xi(\vec{x}')\rangle = \delta_{\vec{x},\vec{x}'}$ ensures that (14) reduces to (12) after averaging over gauge field configurations. So in the random wall source approach one calculates the light quark propagator $G_{\chi,l}$ using the source $\frac{1}{\sqrt{L^3}}\sum_{\vec{x}'}\xi(\vec{x}')$ and $G_{\chi,s}$, the strange propagator by using the source $\frac{1}{\sqrt{L^3}}\sum_{\vec{x}}\xi(\vec{x})e^{i\vec{p}_K\cdot\vec{x}}$. Only one light quark inversion is required in addition to a separate strange quark inversion for each $\vec{p}_K$. In this way one obtains the random wall propagators,

$$G^{rw}_{\chi,l}(y,t_0) \equiv \frac{1}{\sqrt{L^3}}\sum_{\vec{x}'}G_{\chi,l}(y,x')\xi(\vec{x}') \tag{15}$$

and

$$G^{rw}_{\chi,s}(z,t_0;\vec{p}_K) \equiv \frac{1}{\sqrt{L^3}}\sum_{\vec{x}}G_{\chi,s}(z,x)\xi(\vec{x})e^{i\vec{p}_K\cdot\vec{x}}. \tag{16}$$

The expression for the three-point correlator becomes

$$C^{3\,\mathrm{pnt}}_{rw}(t_0,t,T,\vec{p}_K) = \sum_{\vec{y}}\sum_{\vec{z}} e^{i\vec{p}_K\cdot\vec{z}}\times\frac{1}{4}\phi(y)\phi(z)$$
$$\times\langle\mathrm{tr}\{G^{rw\dagger}_{\chi,s}(z,t_0;\vec{p}_K)G_{\chi,c}(z,y)$$
$$\times G^{rw}_{\chi,l}(y,t_0)\}\rangle. \tag{17}$$

The charm propagator in Eq. (17) is obtained by inverting at time slice $y_0 = t_0 - T$ with source $\sum_{\vec{y}}\phi(y)G^{rw}_{\chi,l}(y,t_0)$. In this way one gets the "sequential" charm propagator,

$$G^{\mathrm{seq}}_{\chi,c}(z,t_0,T) \equiv \sum_{\vec{y}}\phi(y)G_{\chi,c}(z,y)G^{rw}_{\chi,l}(y,t_0), \tag{18}$$

and

$$C^{3\,\mathrm{pnt}}_{rw}(t_0,t,T,\vec{p}_K) = \sum_{\vec{z}} e^{i\vec{p}_K\cdot\vec{z}}\times\frac{1}{4}\phi(z)\langle\mathrm{tr}\{G^{rw\dagger}_{\chi,s}(z,t_0;\vec{p}_K)$$
$$\times G^{\mathrm{seq}}_{\chi,c}(z,t_0,T)\}\rangle. \tag{19}$$

The most costly part of our simulations is calculating the random wall strange quark propagators of Eq. (16). A separate inversion is required for each $\vec{p}_K$ [e.g. 8 inversions for the different combinations $(\pm1,\pm1,\pm1)$]. On the other hand, when we change the T values, only $G^{\mathrm{seq}}_{\chi,c}$ of Eq. (18) needs to be recalculated and one inversion suffices for all momenta. This is one of the reasons why the full kaon momentum $\vec{p}_K$ is put into (16) and none into (15).

In Fig. 4 we show comparisons of percentage errors in three-point correlator data of local sources versus random wall sources. One sees significant improvement coming from random wall sources. These tests were carried out in

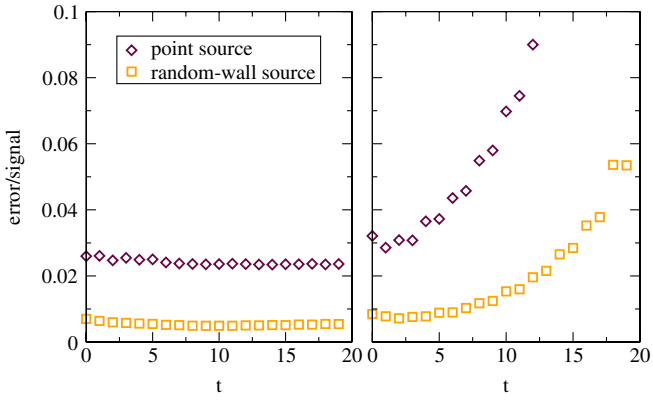

FIG. 4 (color online). Comparison between local and random wall sources for $\vec{p} = \frac{2\pi}{La}(0, 0, 0)$ (left plot), and for $\vec{p} = \frac{2\pi}{La} \times (1, 1, 1)$ (right plot).

the test case $D_s \to \eta_s$, $l\nu$ calculations and with less than the full statistics. For $D \to K$, $l\nu$ we immediately went to random wall sources.

In addition to the three-point correlators, as we will show in the next section, several two-point correlators are needed in order to extract the matrix element $\langle K|S|D\rangle$. They are

$$C_D^{2\,\mathrm{pnt}}(t, t_0) = \frac{1}{L^3}\sum_{\vec{x}}\sum_{\vec{y}}\langle\Phi_D(\vec{y}, t)\Phi_D^\dagger(\vec{x}, t_0)\rangle, \tag{20}$$

and

$$C_K^{2\,\mathrm{pnt}}(t, t_0; \vec{p}_K) = \frac{1}{L^3}\sum_{\vec{x}}\sum_{\vec{y}} e^{i\vec{p}_K\cdot(\vec{x}-\vec{y})}\langle\Phi_K(\vec{y}, t)\Phi_K^\dagger(\vec{x}, t_0)\rangle. \tag{21}$$

The $\frac{1}{L^3}\sum_{\vec{x}}$ can again be implemented via random wall sources. As already mentioned in the previous section, we also calculated correlators for the η_c, η_s, and D_s mesons in exactly the same way as $C_{D/K}^{2\,\mathrm{pnt}}$ in order to carry out and check mass tunings. We have accumulated simulation data for the three- and two-point correlators described in this section for the ensembles of Table I. In the next section we explain how hadronic matrix elements such as $\langle K|S|D\rangle$ and meson masses and decay constants are extracted from this data.

V. FITS AND DATA ANALYSIS

The interpolating operators Φ_D and Φ_K do not create just the ground state D meson or kaon that we are interested in, but they also create excited states with the same quantum numbers. With staggered quarks there is the further complication that in addition to regular states so-called "parity partner" states can contribute, whose energies are measured relative to $i\pi$ so that $e^{-Et} \to (-1)^t e^{-Et}$. The D meson correlator, for instance, has the t dependence (we set $t_0 = 0$ for simplicity),

$$C_D^{2\,\mathrm{pnt}}(t) = \sum_{j=0}^{N_D-1} b_j^D(e^{-E_j^D t} + e^{-E_j^D(N_t-t)}) + \sum_{k=0}^{N_D'-1} d_k^D(-1)^t(e^{-E_k'^D t} + e^{-E_k'^D(N_t-t)}). \tag{22}$$

We are interested in the ground state D meson contribution with amplitude,

$$b_0^D \equiv \frac{|\langle\Phi_D|D\rangle|^2}{2M_D a^3}. \tag{23}$$

Similar relations apply for other mesons. Only in the case of equal mass mesons (π, η_s or η_c) at zero momentum are the oscillatory contributions absent. The three-point correlators such as Eq. (19) will have contributions from regular and oscillatory states for both the kaon and the D meson. The rather complicated t and T dependence is then given by

$$C^{3\,\mathrm{pnt}}(t, T) = \sum_j^{N_K-1}\sum_k^{N_D-1} A_{jk}e^{-E_j^K t}e^{-E_k^D(T-t)} + \sum_j^{N_K-1}\sum_k^{N_D'-1} B_{jk}e^{-E_j^K t}e^{-E_k'^D(T-t)}(-1)^{(T-t)} + \sum_j^{N_K'-1}\sum_k^{N_D-1} C_{jk}e^{-E_j'^K t}e^{-E_k^D(T-t)}(-1)^t + \sum_j^{N_K'-1}\sum_k^{N_D'-1} D_{jk}e^{-E_j'^K t}e^{-E_k'^D(T-t)}(-1)^t(-1)^{(T-t)}. \tag{24}$$

We will only consider the region $0 \le t \le T$ and take $T \ll N_t$ so that any contributions from mesons propagating "around the lattice" due to periodic boundary conditions in time can be neglected. The relevant amplitude here is

$$A_{00} \equiv \frac{\langle\Phi_K|K\rangle\langle K|S|D\rangle\langle D|\Phi_D\rangle}{(2E_K a^3)(2M_D a^3)}a^3. \tag{25}$$

From Eqs. (5) and (23), one sees that our sought after hadronic matrix element is given by

$$\langle K|S|D\rangle = 2\sqrt{M_D E_K}\frac{A_{00}}{\sqrt{b_0^K b_0^D}}. \tag{26}$$

So our goal is to extract the combination on the right-hand side of (26) as accurately as possible and with any

correlations among the errors of the individual components, A_{00}, $b_0^{K/D}$, M_D, and E_K taken properly into account.

We have carried out simultaneous fits to $C_D^{2\,\mathrm{pnt}}$, $C_K^{2\,\mathrm{pnt}}$ and the three-point correlators with different T values, $C^{3\,\mathrm{pnt}}(t, T_i)$ $i = 1, 2 \cdots$. following the fit ansatz of Eqs. (22) and (24). Two (three) different T values are used for the coarse (fine) ensembles. This allows us to evaluate (26) within one fit. The two-point correlators were fit for t values between $t_{\mathrm{min}} = 2(2)$ and $t_{\mathrm{max}} = 30(20 \sim 30)$ for the K and D, respectively, for coarse lattices. For fine lattices, t values were used between $t_{\mathrm{min}} = 2 \sim 4(2)$ and $t_{\mathrm{max}} = 30(30)$. For the three-point correlators, we used all the data between $t = 2$ and $t = T - 2$ for coarse lattices, and $t = 3$ and $t = T - 2$ for fine lattices. Simultaneous fits with multiple T and taking different fit ranges for different correlators were also helpful to reduce the statistical errors, since it allows us to extract maximum information from both the three-point and two-point correlators. The number of exponentials in our fit ansatz was varied to test for stability of fit results. For our final fits, we ended up choosing around $3 \sim 4$ for N_D and N_K. $N'_{D/K}$ was taken to be mostly $N_{D/K} - 1$. Figures 5–9 show some results for A_{00}, M_D, b_0^D, E_K, b_0^K versus N_D or N_K for ensemble C1 at kaon momentum $\vec{p} = (0, 0, 0)$. All our fits are carried out using Bayesian methods [18]. We describe choices for priors and prior widths in the Appendix.

We have found that using data from several $C^{3\,\mathrm{pnt}}$ with different T values helps greatly in reducing statistical/fitting errors. Figure 10 compares results for $f_0(q^2)$ for ensemble C2. One sees that having two rather than just one $C^{3\,\mathrm{pnt}}(t, T_i)$ involved in the simultaneous fit reduces errors and that this effect is most pronounced when one combines an even T with an odd T. It may not be surprising that improvements are achieved from multi-T fits. From the fit ansatz (24), one sees that having more $C^{3\,\mathrm{pnt}}$'s does not increase the number of fit parameters (A_{jk} etc.), although the amount of data and hence of information given to the minimizer is increased. Furthermore,

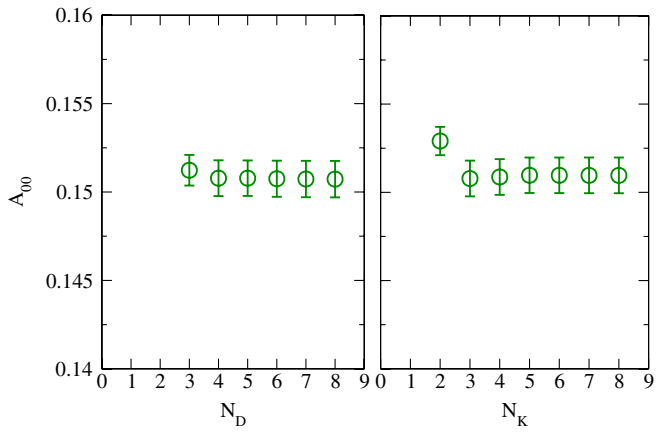

FIG. 5 (color online). A_{00} versus the number $N_{D/K}$. In the left (right) plot N_K (N_D) is fixed at 3 (4).

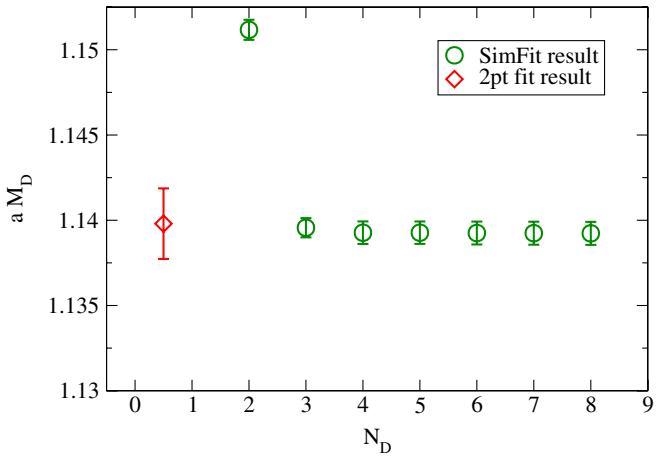

FIG. 6 (color online). aM_D versus N_D. Green circles are from simultaneous $C^{2\,\mathrm{pnt}} - C^{3\,\mathrm{pnt}}$ fits. The red diamond is from fits to just the $C^{2\,\mathrm{pnt}}$.

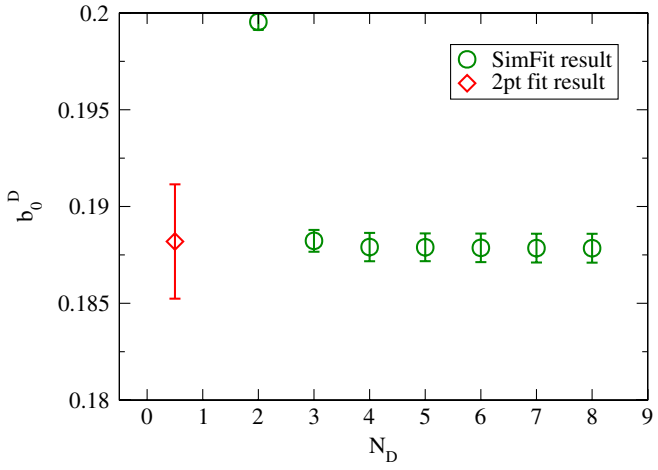

FIG. 7 (color online). Same as Fig. 6 for b_0^D.

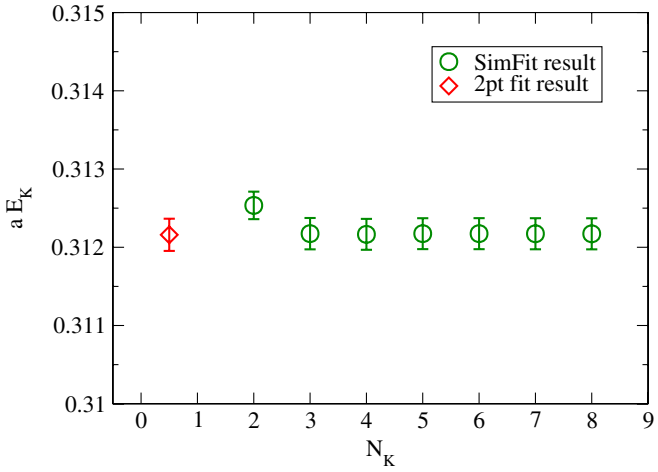

FIG. 8 (color online). Same as Fig. 6 for aE_K versus N_K.

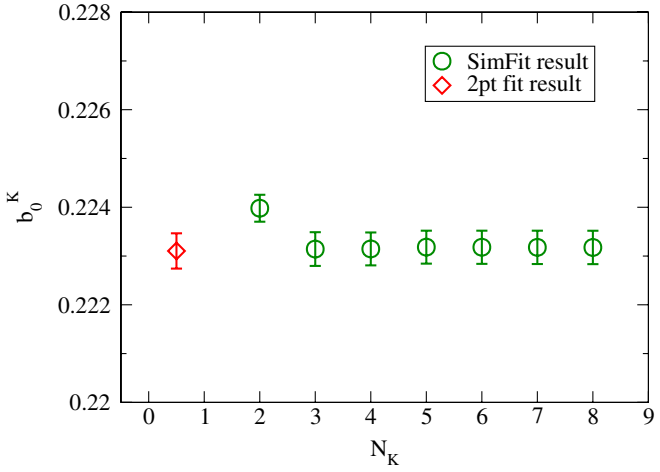

FIG. 9 (color online). Same as Fig. 6 for b_0^K versus N_K.

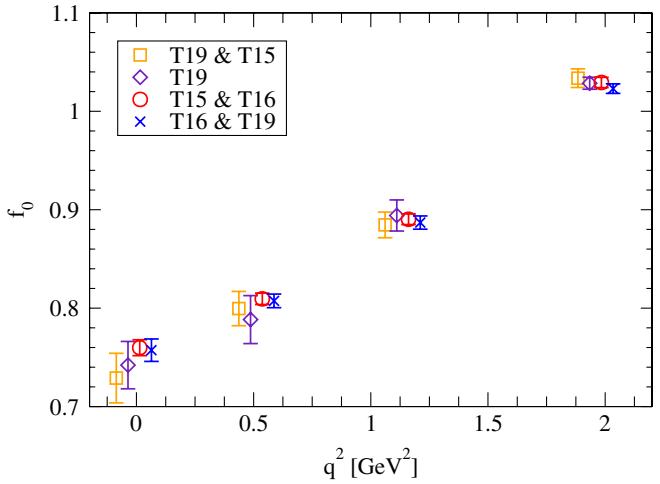

FIG. 10 (color online). Effect of multi-T fits.

if $T_1 + T_2$ is odd, then $(-1)^{T_1 - t}$ and $(-1)^{T_2 - 1}$ have opposite signs and $C^{3\,\mathrm{pnt}}(t, T_1)$ and $C^{3\,\mathrm{pnt}}(t, T_2)$ will provide more independent information.

Most of the fit parameters such as M_D or b_0^D etc. that one gets from the simultaneous $C^{2\,\mathrm{pnt}}$—$C^{3\,\mathrm{pnt}}$ fits can also be determined by just fitting the two-point correlators by themselves. Results from the $C^{2\,\mathrm{pnt}}$ fits are also shown on Figs. 6–9 and provide consistency checks. One interesting outcome is that two-point correlator parameters are more accurately determined via simultaneous fits with three-point correlators than when they are fit alone. This is especially noticeable for D meson correlators, namely, for M_D and b_0^D and has implications for determinations of the decay constant f_D. The latter is related to b_0^D through

$$af_D = \frac{m_{0,c} + m_{0,l}}{M_D}\sqrt{\frac{2b_0^D}{aM_D}}. \tag{27}$$

In Figs. 11 and 12 we compare results for M_D and f_D using either pure two-point fits or simultaneous fits. One sees the

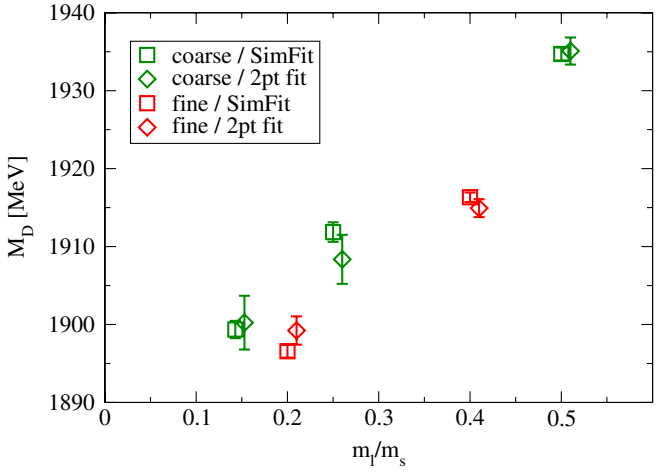

FIG. 11 (color online). Comparison of M_D from two-point and simultaneous fits.

significant improvement coming from the simultaneous fit. Doing simultaneous fits gives a better handle on excited state contributions because they contribute differently to two-point and three-point correlators. This is effectively similar to adding smearings to the correlators. In Sec. VIII we will discuss extracting f_D in the chiral/continuum limit. Having simultaneous fit results will make this determination more accurate than what can be achieved from pure two-point correlators. This appears to be a bonus side product of semileptonic decay studies.

In Tables III, IV, and V we summarize our main fit results. One sees from Table V that we were able to determine $f_0(\vec{p}_K)$ with errors ranging from $\sim$0.2% at zero momentum to $\sim$0.9% at our highest momentum. In Fig. 13 we plot the square of the "speed of light" $c^2(\vec{p})$ for the kaon:

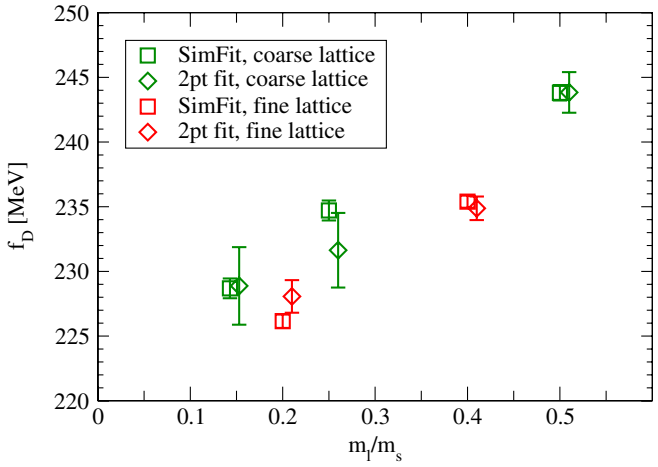

FIG. 12 (color online). Comparison of f_D from two-point and simultaneous fits.

TABLE III. Fit results for aM_D, af_D, aM_{D_s}, and af_{D_s}. Numbers in brackets are from two-point fits, whereas the rest come from simultaneous fits.

Set	aM_D	af_D	aM_{D_s}	af_{D_s}
C1	1.1393(7)	0.1372(4)		
	(1.1398(21))	(0.1373(18))	(1.1876(5))	(0.1539(6))
C2	1.1595(8)	0.1423(4)		
	(1.1574(19))	(0.1405(17))	(1.2008(6))	(0.1560(7))
C3	1.1618(5)	0.1464(3)		
	(1.1620(10))	(0.1464(9))	(1.1899(5))	(0.1553(4))
F1	0.8141(3)	0.0971(2)		
	(0.8152(8))	(0.0979(5))	(0.8473(2))	(0.1083(2))
F2	0.8197(3)	0.1007(2)		
	(0.8191(5))	(0.1005(4))	(0.8435(2))	(0.1078(2))

TABLE IV. Fit results for aM_K, $aE_K(\vec{p})$, af_K, am_π, and af_π. Numbers in brackets are from two-point fits, whereas the rest come from simultaneous fits.

Set	aM_K	aE_K (1,0,0)	aE_K (1,1,0)	aE_K (1,1,1)
C1	0.3122(2)	0.4081(7)	0.4837(9)	0.5469(20)
	(0.3122(2))	(0.4083(7))	(0.4842(9))	(0.5477(24))
C2	0.3285(5)	0.4531(16)	0.5525(17)	0.6373(32)
	(0.3285(3))	(0.4536(13))	(0.5532(18))	(0.6382(33))
C3	0.3572(2)	0.4750(9)	0.5720(10)	0.6524(22)
	(0.3572(2))	(0.4755(9))	(0.5722(11))	(0.6524(35))
F1	0.2285(2)	0.3203(7)	0.3919(9)	0.4559(15)
	(0.2286(2))	(0.3185(12))	(0.3896(23))	(0.4506(47))
F2	0.2460(1)	0.3340(4)	0.4014(7)	0.4609(11)
	(0.2458(2))	(0.3334(7))	(0.4015(10))	(0.4616(16))

Set	af_K	am_π	af_π
C1	0.1011(1)		
	(0.1011(1))	(0.1599(2))	(0.0893(1))
C2	0.1044(1)		
	(0.1045(1))	(0.2108(2))	(0.0949(1))
C3	0.1079(1)		
	(0.1079(1))	(0.2931(2))	(0.1023(1))
F1	0.0721(1)		
	(0.0721(1))	(0.1344(2))	(0.0645(1))
F2	0.0748(1)		
	(0.0747(1))	(0.1873(1))	(0.0697(1))

TABLE V. Fit results for $f_0(\vec{p}_K)$.

Set	$f_0(0, 0, 0)$	$f_0(1, 0, 0)$	$f_0(1, 1, 0)$	$f_0(1, 1, 1)$
C1	1.022(3)	0.916(3)	0.846(3)	0.794(6)
C2	1.023(4)	0.885(5)	0.807(4)	0.758(7)
C3	1.010(2)	0.883(3)	0.803(4)	0.754(5)
F1	1.019(2)	0.876(3)	0.796(3)	0.745(4)
F2	1.011(1)	0.874(2)	0.792(2)	0.739(4)

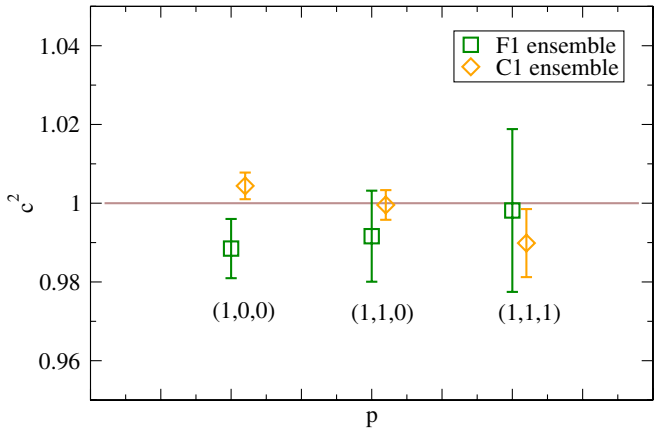

FIG. 13 (color online). Speed of light squared versus momentum for the kaon from the two-point fit.

$$c^2(\vec{p}) = \frac{E_K^2(\vec{p}) - M_K^2}{\vec{p}^2}. \tag{28}$$

One sees that the relativistic dispersion relation is satisfied to about $1 \sim 2\%$. We will check the effect of deviations from exact continuum dispersion relations on our final results for form factors in later sections.

VI. CHIRAL AND CONTINUUM EXTRAPOLATIONS USING THE z EXPANSION

The 20 entries in Table V summarize our results for the form factor $f_0(q^2)$ evaluated on the five ensembles of Table I with four different momenta $\vec{p}_K$ (including zero momentum) per ensemble. The kaon energy in the D rest frame, E_K, is related to q^2 via

$$q^2 = M_D^2 + M_K^2 - 2M_D E_K, \tag{29}$$

and the physical region is $0 \le q^2 \le q^2_{\rm max} = (M_D - M_K)^2$. M_K, E_K, and M_D are given for the different ensembles in Tables III and IV. The next step is to extrapolate the data of Table V to the chiral/continuum physical limit. As is well known, chiral extrapolations for form factors are much more subtle than for static quantities such as masses or decay constants. The main reason for this is that form factors depend not only on meson/quark masses, but also on a kinematic variable such as q^2 (or equivalently on E_K). Kinematic variables are themselves functions of meson masses. It is not sufficient to parametrize just the light quark mass dependence of form factors. One must at the same time capture the kinematic variable dependence correctly for each value of the light quark mass and the lattice spacing (i.e. for each of our ensembles). Furthermore, we are interested in a parametrization that works over the entire physical kinematic range. In the chiral limit, q^2 ranges between $0 \le q^2 \le 1.9$ GeV^2 and E_K between $0.495 \le E_K \le 1.0$ GeV.

A. The z expansion

In addition to q^2 and E_K, a third kinematic variable has proven to be convenient in semileptonic form factor studies, in particular, in recent analysis of $B \to \pi, l\nu$ decays [13–15]:

$$z(q^2, t_0) = \frac{\sqrt{t_+ - q^2} - \sqrt{t_+ - t_0}}{\sqrt{t_+ - q^2} + \sqrt{t_+ - t_0}}, \tag{30}$$

where $t_\pm = (M_D \pm M_K)^2$ and t_0 is a free parameter that defines the zero of the z variable, $z(q^2 = t_0, t_0) = 0$. By going to the z variable, one is mapping the cut region $t_+ < q^2 < \infty$ in the complex q^2 plane onto the circle $|z| = 1$ and $-\infty < q^2 < t_+$ onto $z \in [-1, 1]$. The physical region $0 \le q^2 \le q^2_{\rm max} = t_-$ corresponds then to an even smaller region around $z = 0$. For instance, for the choice $t_0 = 0.5 t_-$ and for physical values of M_D and M_K, one has $-0.057 \le z \le 0.046$. In other words one always has $|z| < 0.06$ in the physical region and this should make z a good variable for a power series expansion. As discussed in the literature using analyticity properties of form factors, one can write

$$f_0(q^2) = \frac{1}{P(q^2)\Phi_0(q^2, t_0)} \sum_{k=0}^{\infty} a_k(t_0) z(q^2, t_0)^k. \tag{31}$$

The function $P(q^2)$ in the denominator is there to factor out any isolated poles in the region $t_- < q^2 < t_+$ below the DK threshold at $q^2 = t_+$. In the case of $D \to K$ semileptonic decays the charm-strange scalar current has the same quantum numbers as the $D^*_{s0}(2317)$ 0^+ meson so that one choice for $P(q^2)$ would be $P(q^2) = (1 - q^2/(M_{D^*_{s0}})^2)$. We have worked with both $P(q^2) = (1 - q^2/(M_{D^*_{s0}})^2)$ and $P(q^2) = 1$ and find that although the expansion coefficients a_k depend on the choice for $P(q^2)$, in either case the data can be reproduced very well with just a few terms (as we will discuss below, with just three terms) in the z expansion.

For the "outer function" Φ_0, we adopt the choice given in Ref. [14]:

$$\Phi_0(q^2, t_0) = \sqrt{\frac{3 t_+ t_-}{32\pi\chi_0}} (\sqrt{t_+ - q^2} + \sqrt{t_+ - t_0}) \times \frac{(t_+ - q^2)^{1/2}}{(t_+ - t_0)^{1/4}} \frac{(\sqrt{t_+ - q^2} + \sqrt{t_+ - t_-})^{1/2}}{(\sqrt{t_+ - q^2} + \sqrt{t_+})^4}. \tag{32}$$

χ_0 has been calculated in the literature using QCD perturbation theory and the operator product expansion. An expression including $\mathcal{O}(\alpha_s)$ and condensate contributions is given for instance in Ref. [14]. For the fixed charm quark mass, χ_0 is a constant and affects just the overall normalization of the a_k's. For simplicity, we ignore the condensate contributions, which are of $\mathcal{O}(m_c^{-3})$ and $\mathcal{O}(m_c^{-4})$, respectively, and retain just the tree-level and $\mathcal{O}(\alpha_s)$ contributions. Any other choice would just mean a common overall rescaling of the expansion coefficients a_k.

B. Testing the z expansion with individual fits

In order to test the usefulness of the z expansion, we first fit $f_0(q^2)$ separately for each individual ensemble using the ansatz of Eq. (31) with $\sum_k \to \sum_{k=0}^{k_{\max}}$. In each case values used for M_D, M_K and hence also for $t_\pm$ were those specific to that ensemble. We employed a common choice for t_0, $t_0 = 0.942$ GeV^2 corresponding to $t_0 = 0.5 \times t_-^{\text{continuum}}$. As is well known from z expansions in general, other choices for t_0 made no difference in resulting fit curves. We find that good individual fits are possible once $k_{\max}$ reaches $k_{\max} = 2$ and that fit curves are then very stable with respect to further increases in $k_{\max}$. In Fig. 14 we show representative results for two ensembles C2 and F1 for $f_0(q^2 = 0)$ versus $k_{\max}$. We also show results for two different choices, $P(q^2) = 1$ and $P(q^2) = (1 - q^2/(M^2_{D^*_{s0}})^2)$. One sees that fit results are very insensitive to these changes in $k_{\max}$ or $P(q^2)$. At finite lattice spacing, we have used $M_{D^*_{s0}} = M_{D_s}^{\text{lattice}} + \delta M$ with $\delta M \equiv [M_{D^*_{s0}}(0^+) - M_{D_s}(0^-)]_{\text{exper}}$. These individual z-expansion fit tests demonstrate (as advocated in the literature) the efficiency of z expansions in capturing the kinematics of form factors with just a small number of parameters and in a model independent way.

In Fig. 15 we give examples of z-expansion fits to individual ensembles, specifically for ensembles C2 and F1.

C. Simultaneous modified z-expansion fit

Having verified the efficacy of the z expansion in fits to individual ensembles, we turn next to modifying the fit ansatz to enable extrapolation to the physical limit. All kinematic properties that depend on q^2 are absorbed by P, Φ_0, and z. A natural way to distinguish between ensembles is to let $a_k \to a_k * D_k$, where D_k contains the light quark mass and lattice spacing dependence as shown below [we set $k_{\max} = 2$ and $P(q^2) = (1 - q^2/(M_{D^*_{s0}})^2)$]:

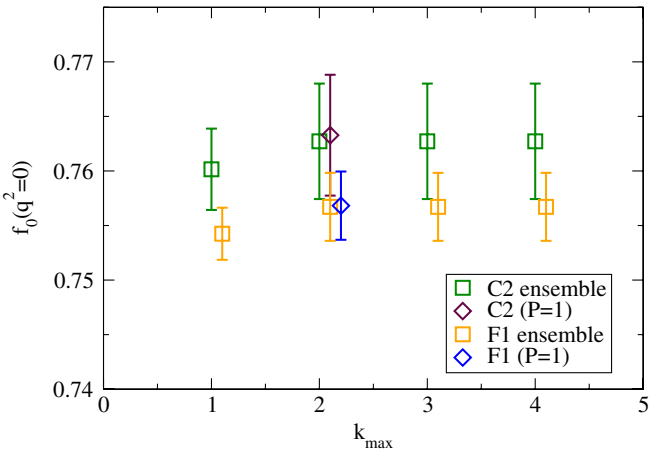

FIG. 14 (color online). $f_0(0)$ versus $k_{\max}$ for ensembles C2 and F1. $P(q^2) = (1 - q^2/(M_{D^*_{s0}})^2)$ everywhere except for at $k_{\max} = 2$ where results for both $P(q^2) = 1$ and $P(q^2) = (1 - q^2/(M_{D^*_{s0}})^2)$ are shown.

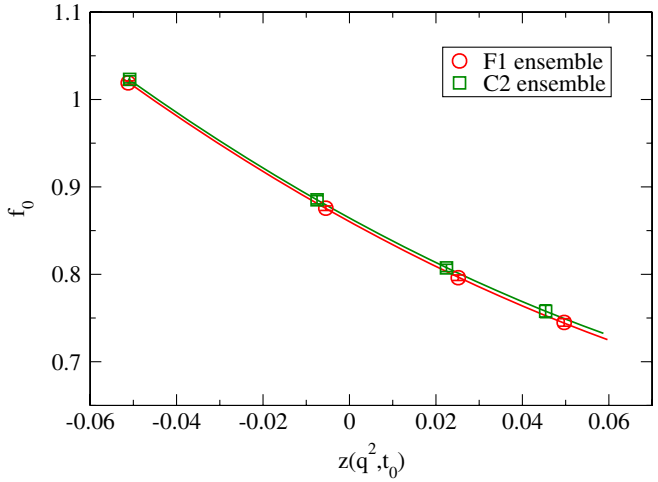

FIG. 15 (color online). Individual z-expansion fits for ensembles C2 and F1.

$$f_0(q^2) = \frac{1}{P(q^2)\Phi_0}(a_0 D_0 + a_1 D_1 z + a_2 D_2 z^2) \times (1 + b_1(aE_K)^2 + b_2(aE_K)^4), \tag{33}$$

where

$$D_i = 1 + c_1^i x_l + c_2^i \delta x_s + c_3^i x_l \log(x_l) + d_i(am_c)^2 + e_i(am_c)^4 + f_i\left(\frac{1}{2}\delta M_\pi^2 + \delta M_K^2\right), \tag{34}$$

$$x_l = \frac{M_\pi^2}{(4\pi f_\pi)^2}, \tag{35}$$

$$\delta x_s = \frac{M_{\eta_s}^2 - M_{\eta_s^{\text{phys}}}^2}{(4\pi f_\pi)^2}, \tag{36}$$

$$\delta M_\pi^2 = \frac{1}{(4\pi f_\pi)^2}((M_\pi^{\text{AsqTad}})^2 - (M_\pi^{\text{HISQ}})^2), \tag{37}$$

$$\delta M_K^2 = \frac{1}{(4\pi f_\pi)^2}((M_K^{\text{AsqTad}})^2 - (M_K^{\text{HISQ}})^2). \tag{38}$$

In Eq. (34), we put typical analytic terms for light valence (x_l and δx_s terms) and sea quark mass (δM_π and δM_K terms) dependence. We quote M_K^{AsqTad} and M_π^{AsqTad} from Ref. [19]. For the chiral logs, we only include up/down quark contributions. The strange quark chiral logs are close to a constant that can be absorbed into the a_i's. There are two distinct sources of lattice spacing dependence. $(am_c)^2$ and $(am_c)^4$ terms are due to the heavy quark discretization error, and $(aE_K)^2$ and $(aE_K)^4$ terms are introduced to estimate the discretization errors due to finite momentum. Since we want the $a_i D_i$ to be independent of the momentum, the aE_K terms are placed separately outside the z expansion. We include lattice spacing dependent terms up to fourth power, however we tested with even higher terms and confirmed that the higher terms are negligible. We have carried out simultaneous fits to all the data of

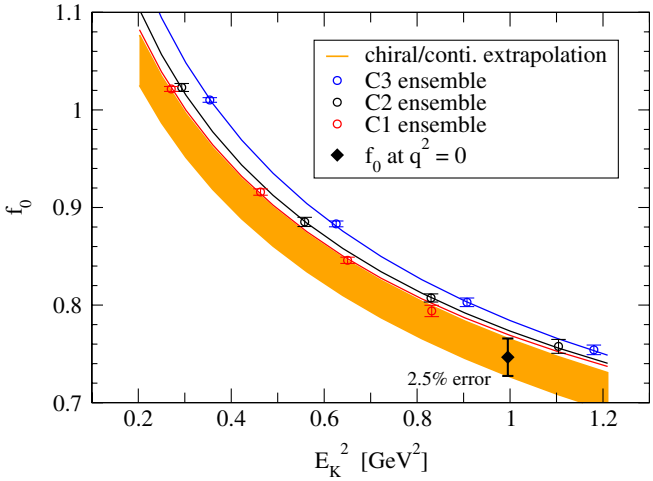

FIG. 16 (color online). Chiral/continuum extrapolation of $f_0(q^2)$ versus E_K^2 from the modified z-expansion ansatz. The data points are coarse lattice points. Three individual curves and the extrapolated band are from a fit to all five ensembles.

Table V using the above ansatz and find that very good fits are possible. Figures 16 and 17 plot the resulting fit curves for each ensemble and the chiral/continuum extrapolated curve with its error band for $f_0(q^2)$ versus E_K^2 (we show separately the coarse and fine ensembles in order to avoid too much clutter). The fit is excellent and has $\chi^2/\mathrm{dof} = 0.44$. In Table VI we summarize fit results for $a_k * D_k$, $k = 0, 1, 2$ coming from the simultaneous fit both for individual ensembles and in the physical limit. These are plotted in Figs. 18–20. In Fig. 21 we plot $f_0(q^2 = 0)$ for the five ensembles and in the physical limit. One sees that within errors this quantity shows little light quark mass dependence and a $\sim$1.3% lattice spacing dependence.

We call the chiral/continuum extrapolation based on the ansatz (33)–(38) and shown in Figs. 16, 17, and 21, the

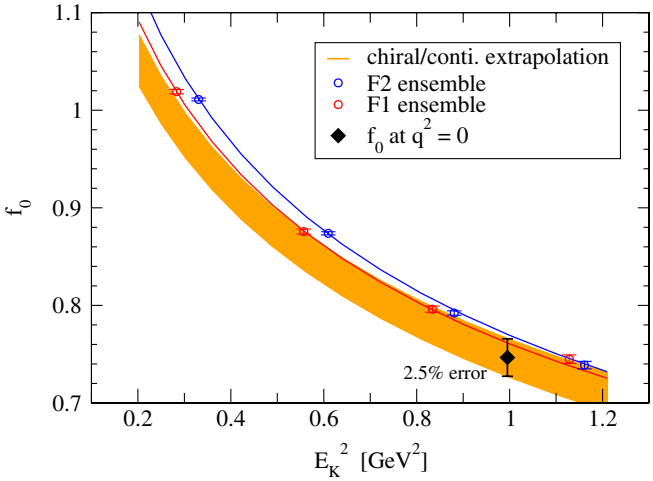

FIG. 17 (color online). Chiral/continuum extrapolation of $f_0(q^2)$ versus E_K^2 from the modified z-expansion ansatz. The data points are fine lattice points. Two individual curves and the extrapolated band are from a fit to all five ensembles.

TABLE VI. The expansion coefficients $a_i * D_i$, $i = 0, 1, 2$ from a simultaneous z-expansion fit to all data.

Set	$a_0 * D_0$	$a_1 * D_1$	$a_2 * D_2$
C1	0.095(2)	0.085(21)	−0.07(11)
C2	0.094(2)	0.083(21)	−0.07(11)
C3	0.089(2)	0.079(21)	−0.07(11)
F1	0.094(1)	0.084(18)	−0.07(11)
F2	0.091(1)	0.080(17)	−0.07(11)
Physical limit	0.097(2)	0.088(18)	−0.07(11)

"simultaneous modified z-expansion extrapolation." We have tested the stability of this extrapolation by adding further terms to the ansatz and/or modifying some of the fit parameters and checking for changes in the physical limit $f_0(q^2 = 0)$. For example, we have

(1) added x_l^2 terms,
(2) modified the lattice spacing dependent terms:
  (a) dropped $(am_c)^4$ and $(aE_K)^4$ terms.
  (b) dropped $(am_c)^4$ term.

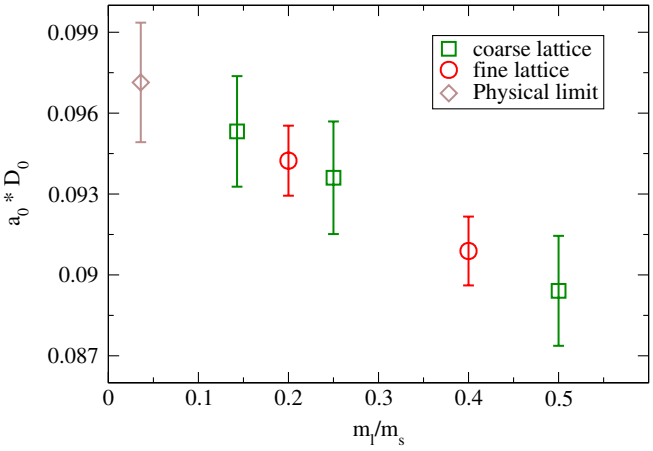

FIG. 18 (color online). The expansion parameter $a_0 * D_0$ versus the light quark mass from a simultaneous fit to all data.

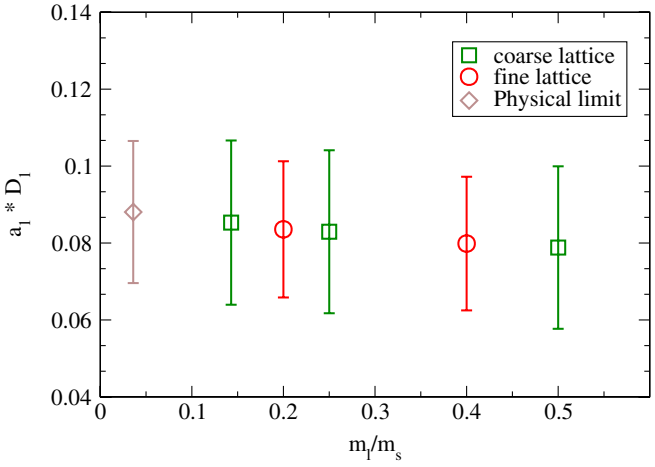

FIG. 19 (color online). Same as Fig. 18 for $a_1 * D_1$.

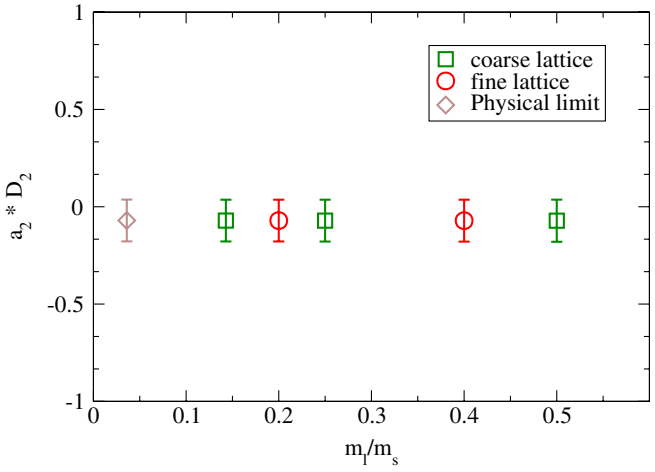

FIG. 20 (color online). Same as Fig. 18 for $a_2 * D_2$.

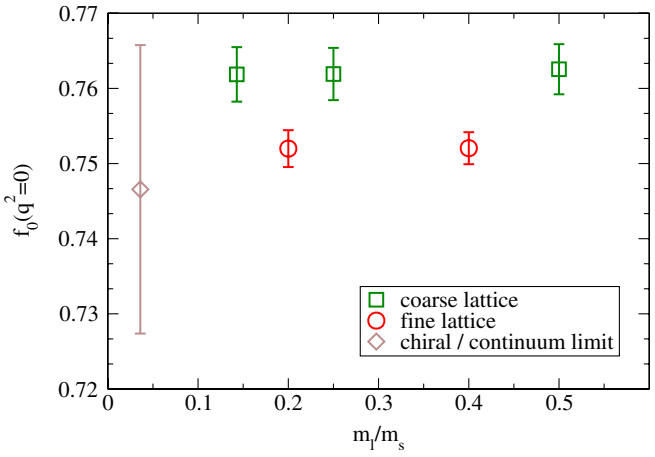

FIG. 21 (color online). f_0 at $q^2 = 0$ for the five ensembles and in the physical limit.

(c) dropped $(aE_K)^4$ term.
(d) added $(am_c)^6$ term.
(e) added up to $(am_c)^{10}$ terms.
(f) added $(aE_K)^6$ term,

(3) used $P(q^2) = 1$ for the pole term,
(4) used E_K from dispersion relations,
(5) used an overall factor $[1 + f(\frac{1}{2}\delta M_\pi + \delta M_K)]$ outside the $\sum_k$ to incorporate sea quark effects, rather than include them in the D_i's,
(6) used an overall factor $[1 + d(am_c)^2 + e(am_c)^4]$ outside the $\sum_k$ to estimate the am_c errors, rather than include them in the D_i's,
(7) replaced $\delta M^2_{\pi/K} \to (M^{\mathrm{AsqTad}}_{\pi/K})^2/(4\pi f_\pi)^2$,
(8) used a simpler $D_i = 1 + d^i_1 x_l + d^i_2 x_s$,
(9) used an even simpler $D_i = 1 + d^i_1 x_l$.

Figure 22 summarizes the results of these tests. One sees that the standard z-expansion extrapolation result is very robust. The second item of the tests checks that we estimate the lattice spacing extrapolation error correctly. Until $(am_c)^4$ and $(aE_K)^4$ terms are included, the error is increasing; however, after including the fourth powers, the error is stabilized. This also shows that the am_c error of the HISQ action is under control in our simulations.

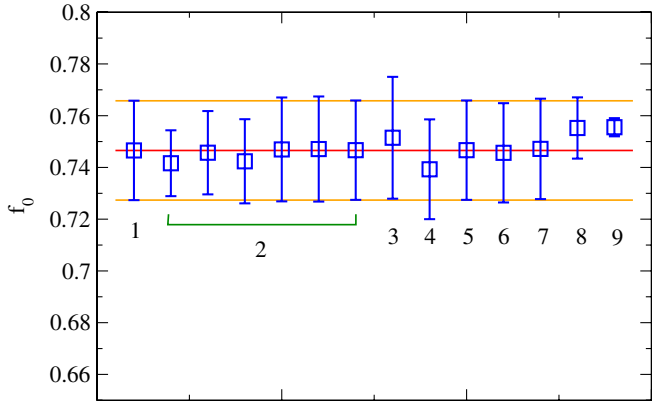

FIG. 22 (color online). Tests of the simultaneous modified z-expansion extrapolation. The red horizontal line is the central value of the fit shown in Figs. 16 and 17, and the orange lines indicate the error. The numbers under the data points correspond to the "test numbers" given in the text.

VII. RESULTS IN THE PHYSICAL LIMIT: $f_+(0)$, $|V_{cs}|$ AND UNITARITY TESTS

This section summarizes the main results of this paper. We present our standard model prediction for the $D \to K$, $l\nu$ decay form factor at $q^2 = 0$, $f_+(0) = f_0(0)$, determine the CKM matrix element $|V_{cs}|$ using input from *BABAR* and CLEO-c and carry out unitarity tests.

A. $f_+(0) = f_0(0)$

We have seen that the simultaneous modified z-expansion extrapolation method gives very stable results. It gives $f_+(0) = 0.748 \pm 0.019$ in the physical limit for $D^0 \to K^- l\nu$, and $f_+(0) = 0.746 \pm 0.019$ for $D^+ \to \bar{K}^0 l\nu$. We take an average over these two channels and our final result in the physical limit becomes

$$f_+^{D\to K}(0) = 0.747 \pm 0.011 \pm 0.015. \qquad (39)$$

The first error comes from statistics and the second error represents systematic errors. Table VII summarizes the error budget. One sees that the largest contributions to the total error come from statistics followed by (am_c) and (aE_K) extrapolation errors.

In order to calculate the form factor, we have to put in meson masses from experiment and also from our lattice simulations. For example, we need experimental D, K, and π meson masses to get the form factor at the physical limit, and E_K, D, and K meson masses from the lattice calculations are used to fit at nonzero lattice spacing. In Table VII, "input meson mass" refers to errors induced

TABLE VII. Total error budget.

Type	Error
Statistical	1.5%
Lattice scale (r_1 and r_1/a)	0.2%
Input meson mass	0.1%
Light quark dependence	0.6%
Strange quark dependence	0.7%
Sea quark dependence	0.4%
am_c extrapolation	1.4%
aE_K extrapolation	1.0%
Finite volume	0.01%
Charm quark tuning	0.05%
Total	2.5%

from these input meson masses. In the fit ansatz, Eq. (34), there are light quark (c_1^i and c_3^i), strange quark (c_2^i), and sea quark dependent terms (f_i). Each systematic error due to these terms is shown on the fourth to sixth line in the table. Lattice spacing dependence errors are estimated separately for $(am_c)^n$ and $(aE_K)^j$ type contributions.

In the fit ansatz, $x_l \log(x_l)$ is the most infrared sensitive term. We calculate the pion-tadpole loop integral both at finite volume and at infinite volume and compare these to estimate the finite volume effects. For the charm quark mass tuning error, we calculate the form factor with a different charm quark mass, $am_c = 0.629$, on the C3 ensemble, and compare with the result with the tuned $am_c = 0.6235$ of Table II. All but the last two entries in Table VII (finite volume and charm mass tuning) were calculated using methods introduced in Ref. [20]. The total error coming out of the chiral/continuum extrapolation can be decomposed into individual contributions, $\sigma^2 = \sum_i c_i \sigma_i^2$, where the sum $\sum_i$ goes over the first 8 entries in Table VII. Details are described in Appendix B.

One might worry about other potential systematic errors, not listed in Table VII, such as those due to missing sea charm quarks or electromagnetism/isospin breaking. The separate numbers given above Eq. (39) for $D^0 \to K^-$ and $D^+ \to \bar{K}^0$ form factors take into account just the differences in masses of the charged versus neutral mesons. This "kinematic" effect is seen to be less than $\sim$0.3%. It is much harder to assess the true dynamical electromagnetic effects. However, no statistically significant differences have been observed experimentally [5], and we will ignore further electromagnetic/isospin breaking effects. Similarly, we will assume that errors due to missing sea charm quarks are small enough so that they do not change the 2.5% total error when added in quadrature. This has been true in the case of several quantities where it was possible and appropriate to apply perturbative estimates of dynamical charm quark effects [21].

The total error for $f_+(0)$ is estimated here to be 2.5%. This is a factor of 4 times smaller than in the previous lattice calculation of Ref. [6]. This was achievable because of applying several new methods and techniques that were described in the text. We employ the HISQ action for both charm and light quark actions and a scalar current rather than the traditional vector current. Because of these new methods, we obtain results with smaller discretization errors and no operator matching. We also developed the modified z-expansion extrapolation method, which is crucial to decrease errors due to the discretization, chiral/continuum extrapolation and parametrization of the form factor. In order to decrease statistical errors, we apply random wall sources and perform simultaneous fits with multiple correlators and T's. If we compare with the error budget of Ref. [6], then we see the statistical errors reduced from 3% to 1.5% and the extrapolation and parametrization errors from 3% to 1.5% as well. The biggest improvement is in the discretization errors. The total discretization errors have now been reduced from 9% to 2%. We note that the concept of the discretization errors is different in Ref. [6] compared to here. In Ref. [6], they estimate the discretization errors by power counting, since they calculate at only one lattice spacing. However, we actually perform continuum extrapolations with correction terms for the discretization effects. As a result, we do not have discretization errors *per se*, but instead extrapolation errors due to higher order correction terms.

In their papers both *BABAR* [4] and CLEO-c [5] have converted their measurements of $f_+(0) * |V_{cs}|$ into results for $f_+(0)$ using values for $|V_{cs}|$ fixed by CKM unitarity. For this CLEO-c uses the 2008 PDG CKM unitarity value of $|V_{cs}| = 0.97334(23)$ [22] and obtains $f_+^{D\to K}(0) = 0.739(9)$ and *BABAR* uses $|V_{cs}| = 0.9729(3)$ leading to $f_+(0) = 0.737(10)$. In Fig. 23 we plot the new HPQCD result of this article, Eq. (39), together with earlier theory results from the lattice [6] and from a recent sum rules calculation [23] and with the *BABAR* and CLEO-c numbers. One sees the very welcome reduction in theory errors which are now small enough so that the agreement between

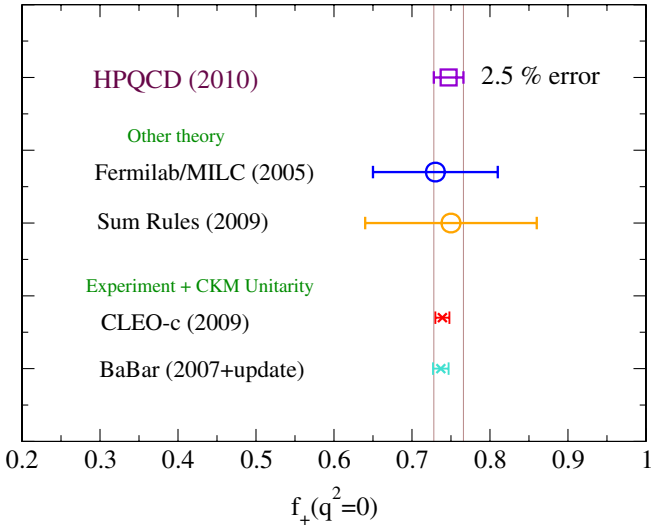

FIG. 23 (color online). Comparisons of $f_0(q^2 = 0)$ with other calculations and experiments.

theory and experiment in Fig. 23 already provides a non-trivial indirect test of CKM unitarity. We can, however, do better and carry out more direct tests of unitarity by determining $|V_{cs}|$ without the assumption of unitarity.

B. Direct determination of $|V_{cs}|$

As experimental input we take $f_+(0) * |V_{cs}| = 0.719(8)$ from CLEO-c [5] and $f_+(0) * |V_{cs}| = 0.717(10)$ from *BABAR* [4]. For the latter we have multiplied *BABAR*'s quoted $f_+(0)$ with their quoted CKM unitarity value for $|V_{cs}|$. Averaging between the two experiments we use $f_+(0) * |V_{cs}| = 0.718(8)$ together with Eq. (39) to extract $|V_{cs}|$. One finds

$$|V_{cs}| = 0.961 \pm 0.011 \pm 0.024, \tag{40}$$

in good agreement (as expected from Fig. 23) with the CKM unitarity value of 0.97345(16) [2]. The first error in (40) is from experiment and the second from the lattice calculation of this article. This is a very precise direct determination of $|V_{cs}|$, made possible by the many advances in lattice QCD that are described in this article together with the tremendous progress in recent experimental studies of D semileptonic decays [4,5]. In Fig. 24 we plot several previous direct determinations of $|V_{cs}|$ from the 2010 PDG [2] together with (40) and the CKM unitarity value.

In a companion paper [21] where we update HPQCD's D_s meson decay constant f_{D_s}, we also determine $|V_{cs}|$ from $D_s \to \tau\nu$ and $D_s \to \mu\nu$ leptonic decays. One finds $|V_{cs}|_{\text{leptonic}} = 1.010(22)$ which is consistent with Eq. (40) at the 1.4σ level.

C. Further unitarity tests

Using the new value of $|V_{cs}|$, Eq. (40), and the current PDG values $|V_{cd}| = 0.230(11)$ and $|V_{cb}| = 0.0406(13)$ one finds

$$|V_{cd}|^2 + |V_{cs}|^2 + |V_{cb}|^2 = 0.978(50) \tag{41}$$

for the 2nd row. And similarly for the 2nd column, with $|V_{us}| = 0.2252(9)$ and $|V_{ts} = 0.0387(21)$ one gets

$$|V_{us}|^2 + |V_{cs}|^2 + |V_{ts}|^2 = 0.976(50). \tag{42}$$

These 2nd row and 2nd column unitarity test results are shown in Fig. 25 together with the PDG numbers mentioned already in the Introduction. Again, one sees the improvement coming from the reduction in the uncertainty in $|V_{cs}|$.

VIII. FURTHER RESULTS FROM TWO-POINT CORRELATORS

In this section we summarize physics results extracted from two-point correlators that emerged as part of our analysis of D meson semileptonic decays. This includes determinations of decay constants, f_π, f_K, f_D, and f_{D_s}. These determinations serve mainly as consistency checks on our quark mass tunings and on our fitting and chiral/continuum extrapolation methods. More extensive studies of f_{D_s} involving five lattice spacings are reported in [21]. Here we present the first results for f_D using HISQ charm and light quarks that employs the new HPQCD r_1 scale [17] (the scale we use throughout in this article).

We use continuum partially quenched chiral perturbation theory (ChPT) formulas augmented by discretization terms to extrapolate to the chiral/continuum limit. Error budgets are close to those in Ref. [10] with, however, a decrease in the r_1 uncertainty. For f_π and f_K, we find

$$f_\pi = 132.3 \pm 1.6 \text{ MeV}, \tag{43}$$

$$f_K = 157.9 \pm 1.5 \text{ MeV}. \tag{44}$$

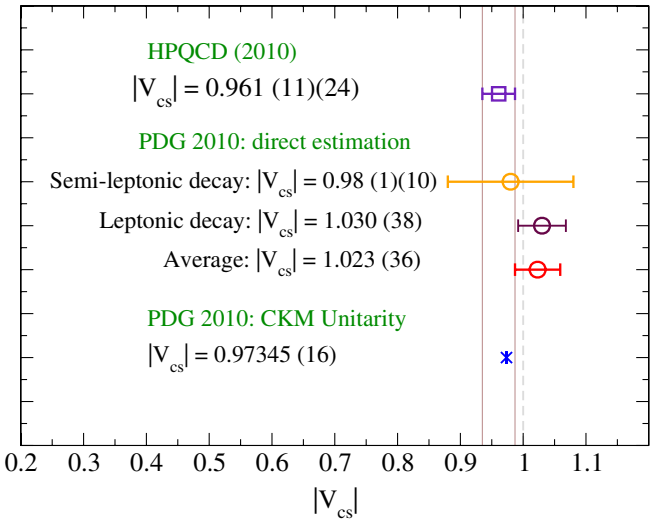

FIG. 24 (color online). Comparisons of our new $|V_{cs}|$ with values in the PDG [2].

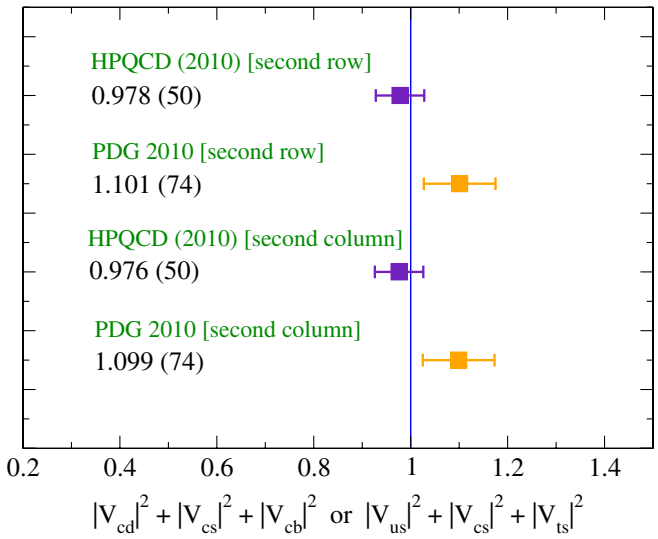

FIG. 25 (color online). Unitarity checks for the second row and second column of the CKM matrix.

One sees that agreement with experimental results summarized in [2] is good and within $1 \sim 1.5\sigma$ (or 1.5%).

For f_D, we have results from the simultaneous fit with three-point correlators and also from just the two-point correlator fits. As we noted in Sec. V, the former has smaller errors however they are consistent with each other:

$$f_D^{\text{SimFit}} = 206.3 \pm 4.3 \text{ MeV}, \tag{45}$$

$$f_D^{\text{2pt}} = 211.1 \pm 5.7 \text{ MeV}. \tag{46}$$

Both values show good agreement with experiment [2] as can be seen in Fig. 26.

For f_{D_s}, we find

$$f_{D_s} = 250.2 \pm 3.6 \text{ MeV}, \tag{47}$$

which agrees with (but is less precise than) our recent update in Ref. [21], $f_{D_s} = 248.0 \pm 2.5$ MeV. One sees that with experimental values having come down in recent years and with the increase in the HPQCD value, there is no longer any discrepancy (beyond 1.6σ) between theory and experiment. The current HFAG [24] number is $f_{D_s} = 257.3 \pm 5.3$ MeV.

Finally, we present the ratio

$$\frac{f_+^{D\to K}(0)}{f_{D_s}} = 2.986 \pm 0.087 \text{ GeV}^{-1}. \tag{48}$$

This quantity can also be obtained from experimental measurements of $D \to K, l\nu$ semileptonic, and D_s leptonic decay branching fractions, and has the virtue that $|V_{cs}|$ drops out in the ratio. We compare (48) with experiment in Fig. 27 and good agreement is found.

IX. SUMMARY AND FUTURE OUTLOOK

We have completed the first study of $D \to K$ semileptonic decays using the HISQ action for the valence charm, strange and light quarks. The most important result of this article is given in Eq. (39) and provides the form factor $f_+^{D\to K}(q^2)$ at $q^2 = 0$. We were able to determine this quantity with a 2.5% total error which represents a four fold improvement in precision over earlier theory results. This is shown in Fig. 23. We then combined our form factor result with recent measurements of $D \to K$ semileptonic decays by the *BABAR* and CLEO-c collaborations to extract a very accurate direct determination of the CKM matrix element $|V_{cs}|$. This is given in Eq. (40) and comparisons with previous determinations shown in Fig. 24. The new value for $|V_{cs}|$ is consistent with the PDG value based on CKM unitarity. We carried out direct tests of 2nd row and 2nd column unitarity with results given in Eqs. (41) and (42) and depicted in Fig. 25. Although still far from the accuracy achieved in 1st row unitarity tests, the reduction in errors on $|V_{cs}|$ has made 2nd row and column unitarity tests much more relevant and interesting than in the past. In Sec. VIII we give a lattice QCD value for $f_+^{D\to K}(0)/f_{D_s}$ which is consistent with experiment. Within the current theory and experimental errors, this provides a highly nontrivial consistency check on how we treat D semileptonic and leptonic decays on the lattice and more generally in the standard model.

The calculations of this article can be improved upon and extended in several ways. The largest errors in Table VII from statistics and continuum extrapolations can be reduced straightforwardly by working with more gauge configurations and time sources and at more values of the lattice spacing. An obvious extension of the current study is to investigate $D \to \pi$ semileptonic decays and determine $|V_{cd}|$. Work on this project has already begun. In a future project we also plan to calculate the vector current hadronic matrix elements $\langle K(\pi)|V_\mu|D\rangle$. This will

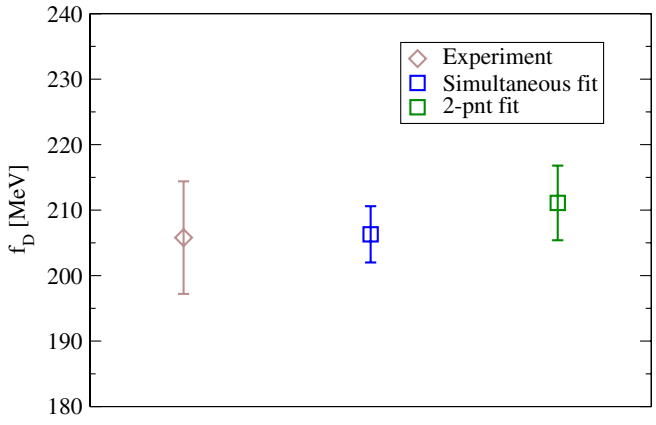

FIG. 26 (color online). Comparisons of f_D with experiment, simultaneous fit, and two-point correlator fit.

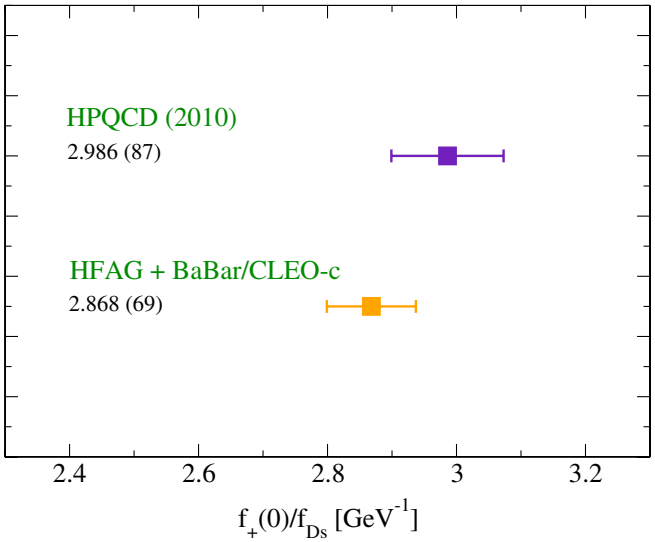

FIG. 27 (color online). Comparisons of $f_+^{D\to K}(0)/f_{D_s}$. We estimate the experiment value from a simple calculation of combining f_{D_s} from HFAG [24] and $f_+^{D\to K}(0)$ from *BABAR* [4] and CLEO-c [5]. This is an appropriate thing to do since both quantities were derived from experimental measurements using the unitarity value of $|V_{cs}|$.

provide $f_+(q^2)$ as a function of q^2. As mentioned in Sec. II we will be carrying out nonperturbative matching of the vector current based on PCVC for this project.

ACKNOWLEDGMENTS

We thank the MILC collaboration for making their AsqTad $N_f = 2 + 1$ configurations available. This work was supported in part by the DOE and NSF in the U.S. and by STFC in the U.K. Computations were carried out at the Ohio Supercomputer Center and on facilities of the USQCD collaboration funded by the Office of Science of the U.S. DOE.

APPENDIX A: PRIORS AND PRIOR WIDTHS FOR SEC. V

We list a sample set of priors and prior widths in Table VIII that have been used for the simultaneous fits to $C_D^{2\,\mathrm{pnt}}$, $C_K^{2\,\mathrm{pnt}}$, and three of the three-point correlators with $T = 19$, 20, and 23 for ensemble F1. The fit ansatz and results have been presented in Sec. V.

APPENDIX B: BAYESIAN FITS IN SEC. VI

From Eqs. (33)–(38), one sees that the chiral/continuum extrapolation ansatz for $f_0(q^2)$ starts out with 23 basic fit parameters c_n, $n = 1, 2, \ldots, 23$:

TABLE VIII. A sample set of the priors and prior widths for ensemble F1 with $\vec{p} = (0, 0, 0)$ and $\vec{p} = (1, 1, 0)$. We have tested with various priors and prior widths, and the fit results are not sensitive to reasonable variations. Note that $i = 1, 2, 3, \ldots$ and j, $k = 0, 1, 2, \ldots$.

	Prior $\vec{p} = (0, 0, 0)$	Width	Prior $\vec{p} = (1, 1, 0)$	Width
A_{jk}	0.01	0.1	0.01	0.1
B_{jk}	0.01	0.1	0.01	0.1
C_{jk}	0.01	0.1	0.01	0.1
D_{jk}	0.01	0.1	0.01	0.1
E_0^D	0.815	$^{+0.815}_{-0.408}$	0.8	$^{+0.8}_{-0.4}$
$E_i^D - E_{i-1}^D$	0.6	$^{+0.6}_{-0.3}$	0.4	$^{+0.4}_{-0.2}$
b_0^D	0.12	1.0	0.015	0.3
b_i^D	0.1	1.0	0.03	0.3
$E_0'^D$	1.0	$^{+1.0}_{-0.5}$	1.0	$^{+1.0}_{-0.5}$
$E_i'^D - E_{i-1}'^D$	0.4	$^{+0.4}_{-0.2}$	0.4	$^{+0.4}_{-0.2}$
d_0^D	0.01	0.1	0.0028	0.1
d_i^D	0.01	0.1	0.006	0.1
E_0^K	0.23	$^{+0.23}_{-0.12}$	0.39	$^{+0.39}_{-0.2}$
$E_i^K - E_{i-1}^K$	0.5	$^{+0.5}_{-0.25}$	0.4	$^{+0.4}_{-0.2}$
b_j^K	0.15	1.0	0.01	0.1
$E_0'^K$	0.4	$^{+0.4}_{-0.2}$	0.53	$^{+0.53}_{-0.27}$
$E_i'^K - E_{i-1}'^K$	0.5	$^{+0.5}_{-0.25}$	0.4	$^{+0.4}_{-0.2}$
d_j^K	0.01	0.1	0.001	0.01

$$c_n\text{: } a_0, a_1, a_2, b_1, b_2, c_1^i, c_2^i, c_3^i, d_i, e_i, f_i, \tag{B1}$$

where $i = 0$, 1, and 2. In a Bayesian fit each of these fit parameters will have its own prior $\bar{c}_n$ and prior width σ_n, which we call "Group I." Our choices for these priors will be discussed below. Our fit ansatz for f_0 includes in addition to the fit parameters c_n also many input parameters such as M_D, E_K, r_1 etc. all of which have some uncertainty associated with them. Ref. [20] describes a method to include effects coming from these types of uncertainties into the final error in the extrapolated value for f_0. What one does is convert all these input parameters into additional fit parameters with priors and prior widths given by their known central values and errors Using this approach we have changed 61 input parameters into new fit parameters p_j, $j = 1, 2, \ldots, 61$, which we call "Group II:"

$$p_j\text{: } \left(\frac{r_1}{a}\right)^i, aM_D^i, aE_K^i(\vec{p}), aM_{\eta_s}^i, aM_\pi^i, (aM_K^{\mathrm{asqtad}})^i, (aM_\pi^{\mathrm{asqtad}})^i,$$
$$M_{D_s^*}^i, r_1, M_{\eta_s}^{\mathrm{phys}}, M_\pi^{\mathrm{phys}}, M_D^{\mathrm{phys}}, M_K^{\mathrm{phys}}, M_{D_s^*}^{\mathrm{phys}}, \tag{B2}$$

where $i = 1, 2, \ldots, 5$ goes over the 5 ensembles. The use of Group II parameters is a very efficient way to include errors coming from uncertainties in input parameters into our final total error. An alternative approach would require visiting each input parameter, in turn, redoing the chiral/continuum extrapolation and coming up with an estimate for the systematic error coming from this input parameter. In our approach no additional systematic errors for these input parameters are called for and the effects from their uncertainties are included in the extrapolation error. For instance, this is very helpful to include the error from E_K^2. In Figs. 16 and 17, there are errors for E_K^2 on the lattice data as well as the extrapolated results, and estimating these errors is not a trivial task. However, introducing the Group II parameters incorporates all E_K^2 errors as part of the final vertical error.

In Bayesian fits one minimizes the augmented chi squared,

$$\chi^2_{\mathrm{aug}} = \chi^2_{\mathrm{traditional}} + \chi^2_{\mathrm{GroupI}} + \chi^2_{\mathrm{GroupII}}, \tag{B3}$$

$$\chi^2_{\mathrm{traditional}} = \sum_{i=1}^{20} \frac{(f_0^i - f_0(\mathrm{ansatz}))^2}{(\sigma_{f_0}^i)^2}, \tag{B4}$$

$$\chi^2_{\mathrm{GroupI}} = \sum_{n=1}^{23} \frac{(c_n - \bar{c}_n)^2}{\sigma_n^2}, \tag{B5}$$

$$\chi^2_{\mathrm{GroupII}} = \sum_{j=1}^{61} \frac{(p_j - \bar{p}_j)^2}{\sigma_j^2}. \tag{B6}$$

When carrying out the chiral/continuum extrapolations, we have expressed all dimensionful quantities in units of GeV. We give the set of priors and prior widths for the Group I parameters c_n in Table IX and for the Group II parameters p_j in Tables X and XI.

Setting priors and prior widths is straightforward. For Group I, the quark mass terms, such as x_l and x_s, are normalized by the scale, $\Lambda \equiv 4\pi f_\pi$. Therefore, it is natural that we expect that the parameters vary between -1 to 1. However, we know from other lattice calculations with the same gauge configurations and our lattice data that the sea quark mass contribution is smaller than that of valence quark. Thus, we take the priors and prior widths for the sea quark mass terms as $f_i = 0 \pm 0.3$. The leading heavy quark error is proportional to $\mathcal{O}(\alpha_s(am_c)^2)$ so we use $d_j = 0 \pm 0.3$ for the $(am_c)^2$ terms. For the purposes of setting priors, we conservatively do not include a factor of v^2/c^2 here. On the other hand for the $(am_c)^4$ terms, we do take the expected factor of v^2/c^2 into account and choose $e_i = 0 \pm 0.2$. Similarly, we use $b_j = 0 \pm 0.3$ for the $(aE_K)^2$ and $(aE_K)^4$ terms. This reflects a factor of α_s for the $(aE_K)^2$ terms and the fact that higher powers of (ap^μ) typically come with smaller numerical factors relative to lower powers [such as in an expansion of $\frac{1}{a}\sinh(aE)$]. For Group II, we use lattice results and experiments that we described in the text for the priors and prior widths.

TABLE IX. Priors and prior width of the Group I parameters for the simultaneous modified z-expansion extrapolation fit.

Group I	Prior	Width	Fit result	Fit error
a_0	0	1	0.09766	0.0029
a_1	0	1	0.08999	0.02
a_2	0	1	−0.07044	0.11
b_1	0	0.3	0.03775	0.13
b_2	0	0.3	0.07179	0.17
c_1^0	0	1	−0.52596	0.31
c_1^1	0	1	−0.19051	0.82
c_1^2	0	1	0.02877	1
c_2^0	0	1	−0.09919	0.98
c_2^1	0	1	0.00827	1
c_2^2	0	1	0.00044	1
c_3^0	0	1	−0.02897	0.24
c_3^1	0	1	0.32804	0.66
c_3^2	0	1	−0.03116	1
d_0	0	0.3	0.00966	0.11
d_1	0	0.3	0.01769	0.29
d_2	0	0.3	0.00541	0.3
e_0	0	0.2	0.01554	0.19
e_1	0	0.2	0.00447	0.2
e_2	0	0.2	0.00131	0.2
f_0	0	0.3	−0.10860	0.28
f_1	0	0.3	−0.00474	0.3
f_2	0	0.3	0.00105	0.3

TABLE X. Priors and prior width of the Group II parameters for the simultaneous modified z-expansion extrapolation fit. Parameters with five rows correspond to that on the five ensembles, C1, C2, C3, F1, and F2.

Group II	Prior	Width	Fit result	Fit error
r_1	0.3133	0.0023	0.313285	0.0023
$M_{\eta_s}^{\rm phys}$	0.6858	0.004	0.685799	0.004
$M_\pi^{\rm phys}$	0.1373	0.0023	0.1373	0.0023
$M_D^{\rm phys}$	1.8645	0.0004	1.8645	0.0004
$M_K^{\rm phys}$	0.4937	0.000016	0.4937	0.000016
$M_{D_s^*}^{\rm phys}$	2.3173	0.0006	2.3173	0.0006
r_1/a	2.647	0.003	2.64677	0.003
	2.618	0.003	2.61818	0.003
	2.644	0.003	2.64388	0.003
	3.699	0.003	3.69905	0.003
	3.712	0.004	3.71213	0.0039
aM_D	1.13927	0.00066	1.13925	0.00066
	1.15947	0.00076	1.15949	0.00076
	1.16179	0.0005	1.16179	0.0005
	0.814062	0.00035	0.814066	0.00035
	0.819663	0.00026	0.819663	0.00026
aE_K	0.312174	0.0002	0.312159	0.0002
$\vec{p} = (0, 0, 0)$	0.32851	0.00048	0.328529	0.00048
	0.357205	0.00022	0.357228	0.00022
	0.228546	0.00017	0.228572	0.00017
	0.24596	0.00014	0.245944	0.00014
aE_K	0.408141	0.00066	0.408059	0.00065
$\vec{p} = (1, 0, 0)$	0.453061	0.0016	0.453098	0.0015
	0.475036	0.00087	0.474849	0.00086
	0.320348	0.00069	0.320396	0.00067
	0.333981	0.00037	0.333932	0.00036
aE_K	0.483702	0.00094	0.483798	0.00093
$\vec{p} = (1, 1, 0)$	0.552504	0.0017	0.552527	0.0016
	0.572004	0.001	0.572016	0.001
	0.391932	0.00087	0.391883	0.00085
	0.401385	0.00065	0.401619	0.00064
aE_K	0.546941	0.002	0.547535	0.002
$\vec{p} = (1, 1, 1)$	0.637288	0.0032	0.637096	0.0032
	0.652424	0.0022	0.652314	0.0022
	0.45593	0.0015	0.455311	0.0015
	0.460897	0.0011	0.460966	0.0011
aM_{η_s}	0.411128	0.00018	0.41113	0.00018
	0.414346	0.00022	0.414345	0.00022
	0.411848	0.00022	0.411847	0.00022
	0.294159	0.00012	0.294158	0.00012
	0.293114	0.00018	0.293117	0.00018
aM_π	0.159893	0.00017	0.159895	0.00017
	0.210815	0.00023	0.210813	0.00023
	0.293124	0.00023	0.293119	0.00023
	0.134449	0.00015	0.134445	0.00015
	0.187346	0.00013	0.18735	0.00013

TABLE XI. (Continued) Priors and prior width of the Group II parameters for the simultaneous modified z-expansion extrapolation fit. Parameters with five rows correspond to that on the five ensembles, C1, C2, C3, F1, and F2. We quote M_K^{AsqTad} and M_π^{AsqTad} from Ref. [19].

Group II	Prior	Width	Fit result	Fit error
aM_K^{asqtad}	0.3653	0.00029	0.365304	0.00029
	0.38331	0.00024	0.383309	0.00024
	0.40984	0.00021	0.409839	0.00021
	0.25318	0.00019	0.253177	0.00019
	0.27217	0.00021	0.272174	0.00021
aM_π^{asqtad}	0.15971	0.0002	0.15971	0.0002
	0.22447	0.00017	0.22447	0.00017
	0.31125	0.00016	0.31125	0.00016
	0.14789	0.00018	0.147889	0.00018
	0.20635	0.00018	0.206351	0.00018
$M_{D_s^*}$	2.32897	0.005	2.33033	0.0047
	2.32899	0.005	2.32818	0.0048
	2.33053	0.005	2.33028	0.0048
	2.32293	0.005	2.32179	0.0045
	2.32113	0.005	2.32197	0.0045

As we stated above, all sources of systematic errors are already included in the fit ansatz, except the finite volume and charm quark mass tuning errors. We can consider the total error squared, σ^2, as a linear combination of each source [20];

$$\sigma^2 = \sum_{n=1}^{23} C_{c_n}\sigma_{c_n}^2 + \sum_{j=1}^{61} C_{p_j}\sigma_{p_j}^2, \tag{B7}$$

where the first term is for Group I (c_n), and the second term is for Group II (p_j). We actually calculate the contributions from each source, $C_{c_n}\sigma_{c_n}^2$ and $C_{p_j}\sigma_{p_j}^2$ using the method presented in [20], and they add up to the total error σ^2 correctly. We group together appropriate parameters, and list them in Table VII.

APPENDIX C: CHIRAL AND CONTINUUM EXTRAPOLATIONS BASED ON CHIRAL PERTURBATION THEORY

In this Appendix we carry out further consistency tests of the chiral/continuum extrapolation of Sec. VI by working with a completely independent fit ansatz. We will use the partially quenched chiral perturbation theory (PQChPT) formulas developed in Refs. [25,26] augmented by terms parametrizing discretization effects and E_K dependence.

Heavy meson ChPT formulas are organized through form factors $f_\parallel$ and $f_\perp$ in terms of which $f_0(q^2)$ is given by

$$f_0(q^2) = \frac{\sqrt{2M_D}}{M_D^2 - M_K^2}[(M_D - M_K)f_\parallel + (E_K^2 - M_K^2)f_\perp]. \tag{C1}$$

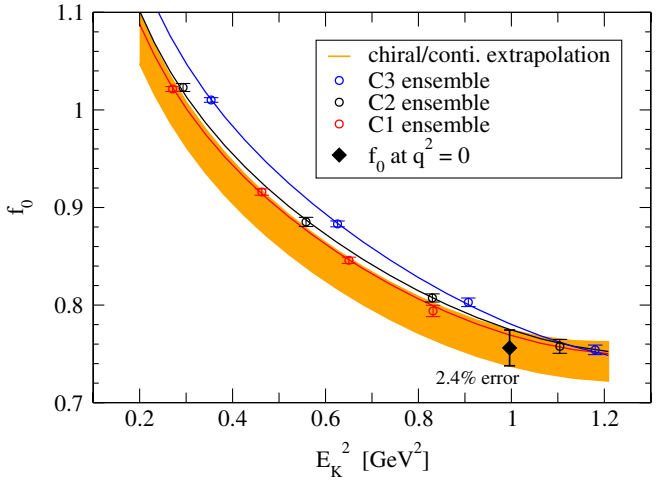

FIG. 28 (color online). Chiral/continuum extrapolation of $f_0(q^2)$ versus E_K^2 from the ChPT ansatz. The data points are coarse lattice points. Three individual curves and the extrapolated band are from a fit to all five ensembles.

We follow very closely the approach and notation of Ref. [26], however with all the taste breaking effects turned off. $f_\parallel$ and $f_\perp$ are parametrized as

$$f_\parallel = \frac{\kappa}{f_\pi}[1 + \delta f_\parallel + c_l^\parallel m_l + c_{s'}^\parallel m_{s'} + c_{\mathrm{sea}}^\parallel(2m_u + m_s) + h_\parallel(E_K)](1 + c_0(am_c)^2 + c_1(am_c)^4), \tag{C2}$$

$$f_\perp = \frac{\kappa}{f_\pi}\frac{g_\pi}{(E_k + \Delta^* + D)}[1 + \delta f_\perp + c_l^\perp m_l + (c_l^\parallel + c_l^\perp - c_{s'}^\parallel)m_{s'} + c_{\mathrm{sea}}^\perp(2m_u + m_s) + h_\perp(E_K)](1 + c_0(am_c)^2 + c_1(am_c)^4). \tag{C3}$$

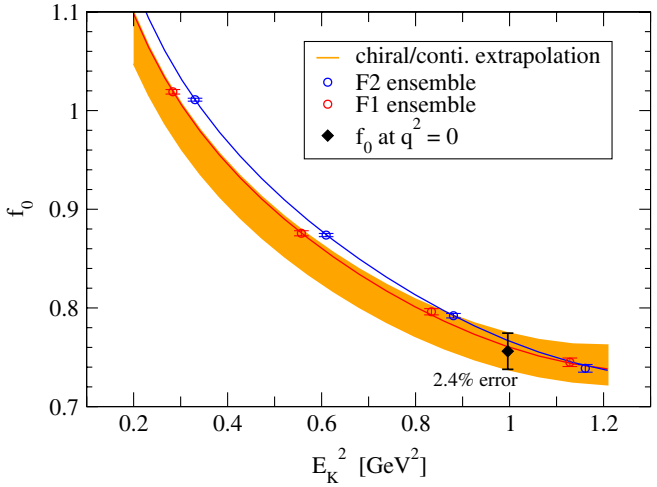

FIG. 29 (color online). Chiral/continuum extrapolation of $f_0(q^2)$ versus E_K^2 from the ChPT ansatz. The data points are fine lattice points. Two individual curves and the extrapolated band are from a fit to all five ensembles.

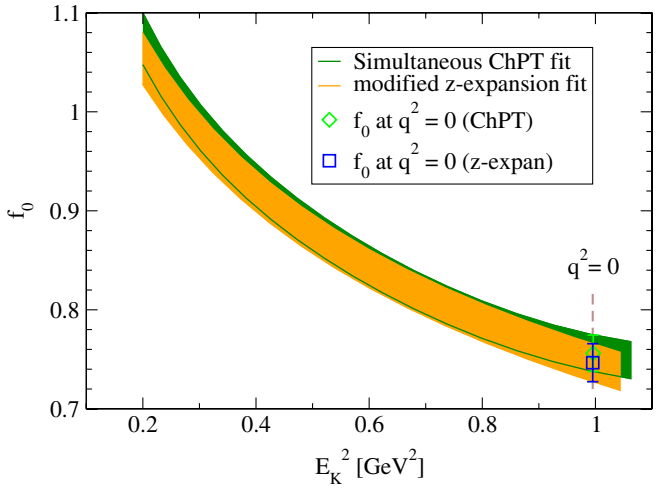

FIG. 30 (color online). Comparisons of $f_0(q^2)$ in the physical limit from the z-expansion and the ChPT extrapolations.

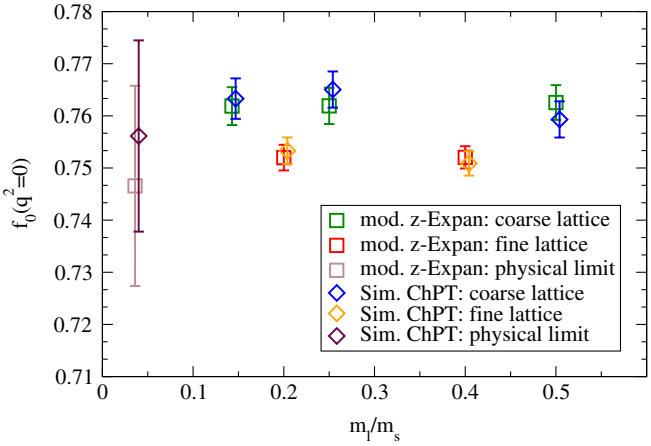

FIG. 31 (color online). Comparisons of f_0 at $q^2 = 0$ for the five ensembles and in the physical limit from the z-expansion and the ChPT extrapolations.

The chiral logs are contained in $\delta f_\parallel$, $\delta f_\perp$, and D. We give their explicit expressions in Appendix D. m_l and $m_{s'}$ are valence and m_u and m_s the sea quark masses. g_π is the $DD^*\pi$ coupling and Δ^* the $D_s^* - D$ mass splitting. $h_\parallel(E_K)$ and $h_\perp(E_K)$ are unknown functions of E_K. We will use polynomial expansions for them. $h_{\parallel,\perp}(E_K) = c_1^{\parallel,\perp} E_K + c_2^{\parallel,\perp} E_K^2 + \cdots$. The first two terms are motivated by ChPT [26], however we view $h_{\parallel,\perp}(E_K)$ as potentially parametrizing f_0 more generally, even beyond the regime of small E_K where ChPT is assumed valid. Our data is fit very well ($\chi^2/\text{dof} = 0.48$), however, all the way to $E_K \approx 1$ GeV keeping just terms through $\mathcal{O}(E_K^2)$ in $h_\parallel$ and $h_\perp$. Figures 28 and 29 show results from a simultaneous fit to all our data points using the ChPT ansatz. These should be compared to Figs. 16 and 17 from the modified z-expansion ansatz.

In Fig. 30 we compare $f_0(q^2)$ in the physical limit coming from the z-expansion extrapolation of Sec. VI and the ChPT extrapolation of this Appendix over the entire physical q^2 range. And in Fig. 31 we compare results at $q^2 = 0$ for each ensemble and in the physical limit. One sees that the two extrapolations are nicely consistent with each other. We believe the consistency check of this Appendix has been very useful. It provides further support for the results of the z-expansion extrapolation and indicates that errors there were not underestimated. Note that the ChPT ansatz includes all the complicated chiral logs of Appendix D, whereas the z-expansion ansatz makes do with just a simple $x_l \log x_l$ term.

APPENDIX D: PARTIALLY QUENCHED CHPT CHIRAL LOGS

In this appendix we summarize partially quenched ChPT (PQChPT) expressions for the chiral logarithm terms $\delta f_\parallel$, $\delta f_\perp$, and D that we employ in Eqs. (C2) and (C3). The formulas for PQChPT in continuum QCD for heavy-to-light semileptonic decays were first developed in Ref. [25] for degenerate sea quarks. Reference [26] generalized these results to nondegenerate $1 + 1 + 1$ sea quarks and also to staggered ChPT. We have started from the $1 + 1 + 1$ continuum PQChPT expressions given in Ref. [26] for individual diagrams and for the D and kaon wave function renormalizations to obtain the full $\delta f_{\parallel,\perp}$ in the $2 + 1$ PQhPT case. For the convenience of the reader, we give these reconstructed expressions below. We use the same notation as in Ref. [26]. "x" and "y" stand for the light valence quarks in the daughter meson (for the kaon $x \equiv l$ and $y \equiv s'$) and "u" and "s" denote sea light and strange quarks. Furthermore, m_{ab} is the mass of the pseudoscalar meson with quark content a and b and $m_\eta^2 = \frac{1}{3}(m_{uu}^2 + 2m_{ss}^2)$:

$$(4\pi f)^2 \delta f_\parallel^{D\to K} = \Big\{\Big[I_1(m_{yu}) + \frac{1}{2} I_1(m_{ys})\Big] - 3g_\pi^2\Big[I_1(m_{xu}) + \frac{1}{2} I_1(m_{xs})\Big] + [2I_2(m_{yu}) + I_2(m_{ys})] + \frac{1}{3}[R_x^{[3,2]}(m_{xx})(I_1(m_{xx}) + I_2(m_{xx})) + R_y^{[3,2]}(m_{yy})(I_1(m_{yy}) + I_2(m_{yy})) + R_\eta^{[3,2]}(m_\eta)(I_1(m_\eta) + I_2(m_\eta))] + \frac{1}{6}[DR^{[2,2]}(m_{yy}; I_1)] - \frac{3g_\pi^2}{6}[DR^{[2,2]}(m_{xx}; I_1)] + \frac{1}{3}[DR^{[2,2]}(m_{yy}; I_2)]\Big\}, \quad \text{(D1)}$$

$$(4\pi f)^2\delta f_{\perp}^{D\to K} = \left\{-\left[I_1(m_{yu}) + \frac{1}{2}I_1(m_{ys})\right] - 3g_\pi^2\left[I_1(m_{xu}) + \frac{1}{2}I_1(m_{xs})\right] - \frac{g_\pi^2}{3}[R_x^{[3,2]}(m_{xx})K_1(m_{xx}) + R_y^{[3,2]}(m_{yy})K_1(m_{yy}) + R_\eta^{[3,2]}(m_\eta)K_1(m_\eta)] - \frac{1}{6}[DR^{[2,2]}(m_{yy};I_1)] - \frac{3g_\pi^2}{6}[DR^{[2,2]}(m_{xx};I_1)]\right\}, \quad \text{(D2)}$$

$$(4\pi f)^2 D^{D\to K} = -3g_\pi^2(v\cdot p)\times\left\{[2K_1(m_{yu}) + K_1(m_{ys})] + \frac{1}{3}[DR^{[2,2]}(m_{yy};K_1)]\right\}. \quad \text{(D3)}$$

In the D meson rest frame $v\cdot p = E_K$. Furthermore, one has

$$I_1(m) = m^2\log\frac{m^2}{\Lambda^2}, \quad \text{(D4)}$$

$$I_2(m) = -2(v\cdot p)^2\log\frac{m^2}{\Lambda^2} - 4(v\cdot p)^2F\left(\frac{m}{v\cdot p}\right) + 2(v\cdot p)^2, \quad \text{(D5)}$$

with

$$F(x) = \begin{cases}\sqrt{1-x^2}\tanh^{-1}(\sqrt{1-x^2}) & 0\le x\le 1\\ -\sqrt{x^2-1}\tan^{-1}(\sqrt{x^2-1}) & x>1\end{cases}, \quad \text{(D6)}$$

$$K_1(m) = \left[-m^2 + \frac{2}{3}(v\cdot p)^2\right]\log\frac{m^2}{\Lambda^2} + \frac{4}{3}[(v\cdot p)^2 - m^2] * F\left(\frac{m}{v\cdot p}\right) - \frac{10}{9}(v\cdot p)^2 + \frac{4}{3}m^2 - \frac{2\pi}{3}\frac{m^3}{v\cdot p}, \quad \text{(D7)}$$

$$R_x^{[3,2]}(m) = \frac{(m_{uu}^2-m^2)(m_{ss}^2-m^2)}{(m_{yy}^2-m^2)(m_\eta^2-m^2)}, \quad \text{(D8)}$$

$$R_y^{[3,2]}(m) = \frac{(m_{uu}^2-m^2)(m_{ss}^2-m^2)}{(m_{xx}^2-m^2)(m_\eta^2-m^2)}, \quad \text{(D9)}$$

$$R_\eta^{[3,2]}(m) = \frac{(m_{uu}^2-m^2)(m_{ss}^2-m^2)}{(m_{xx}^2-m^2)(m_{yy}^2-m^2)}, \quad \text{(D10)}$$

$$R^{[2,2]}(m;\mathcal{I}) = \frac{(m_{uu}^2-m^2)(m_{ss}^2-m^2)}{(m_\eta^2-m^2)}\mathcal{I}(m) + \frac{(m_{uu}^2-m_\eta^2)(m_{ss}^2-m_\eta^2)}{(m^2-m_\eta^2)}\mathcal{I}(m_\eta), \quad \text{(D11)}$$

and

$$DR^{[2,2]}(m;\mathcal{I}) = \frac{\partial}{\partial m^2}R^{[2,2]}(m;\mathcal{I}). \quad \text{(D12)}$$

We refer the reader to the original literature [25,26] for further details. Here, for completeness, we give partially quenched formulas for the chiral logarithms in $D\to\pi$ decays. They will be used shortly in our own studies of $D\to\pi, l\nu$ decays. Some care is required in taking the $y\to x$ limit of (D1)–(D3), however in the end expressions are simpler for $D\to\pi$ than for $D\to K$:

$$(4\pi f)^2\delta f_{\parallel}^{D\to\pi} = \left\{(1-3g_\pi^2)\left[I_1(m_{xu}) + \frac{1}{2}I_1(m_{xs})\right] + [2I_2(m_{xu}) + I_2(m_{xs})] - \frac{1+3g_\pi^2}{6}[DR^{[2,2]}(m_{xx};I_1)]\right\}, \quad \text{(D13)}$$

$$(4\pi f)^2\delta f_{\perp}^{D\to\pi} = \left\{-(1+3g_\pi^2)\left[I_1(m_{xu}) + \frac{1}{2}I_1(m_{xs})\right] + \frac{g_\pi^2}{3}[DR^{[2,2]}(m_{xx};K_1)] - \frac{1+3g_\pi^2}{6}[DR^{[2,2]}(m_{xx};I_1)]\right\}, \quad \text{(D14)}$$

$$(4\pi f)^2 D^{D\to\pi} = -3g_\pi^2(v\cdot p)\times\left\{[2K_1(m_{xu}) + K_1(m_{xs})] + \frac{1}{3}[DR^{[2,2]}(m_{xx};K_1)]\right\}. \quad \text{(D15)}$$

[1] M. Antonelli *et al.* (FlaviaNet Working Group on Kaon Decays), Eur. Phys. J. C **69**, 399 (2010).

[2] K. Nakamura *et al.* (Particle Data Group), J. Phys. G **37**, 075021 (2010).

[3] L. Widhalm *et al.* (Belle Collaboration), Phys. Rev. Lett. **97**, 061804 (2006).

[4] B. Aubert *et al.* (*BABAR* Collaboration), Phys. Rev. D **76**, 052005 (2007); P. Roudeau (private communication).

[5] D. Besson *et al.* (CLEO Collaboration), Phys. Rev. D **80**, 032005 (2009).

[6] C. Aubin *et al.* (Fermilab Lattice, MILC, and HPQCD Collaborations), Phys. Rev. Lett. **94**, 011601 (2005).

[7] J. Bailey *et al.* (Fermilab Lattice and MILC Collaborations), Proc. Sci. LAT2009 (**2009**) 250; , arXiv:1011.2423.

[8] E. Follana *et al.* (HPQCD Collaboration), Phys. Rev. D **75**, 054502 (2007).

[9] S. Simula *et al.* (ETM Collaboration), Proc. Sci. LAT2009 (**2009**) 257.

[10] E. Follana *et al.* (HPQCD Collaboration), Phys. Rev. Lett. **100**, 062002 (2008).

[11] H. Na *et al.* (HPQCD Collaboration) Proc. Sci. LAT2009 (2009) 247.

[12] A. Bazavov *et al.* (MILC Collaboration), Rev. Mod. Phys. **82**, 1349 (2010).

[13] C. G. Boyd, B. Grinstein, and R. F. Lebed, Phys. Rev. Lett. **74**, 4603 (1995).L. Lellouch, Nucl. Phys. **B479**, 353 (1996).

[14] M. C. Arnesen *et al.*, Phys. Rev. Lett. **95**, 071802 (2005).

[15] T. Becher and R. J. Hill, Phys. Lett. B **633**, 61 (2006).

[16] S. Naik, Nucl. Phys. **B316**, 238 (1989); G. P. Lepage, Phys. Rev. D **59**, 074502 (1999); K. Orginos *et al.*, *ibid.* **60**, 054503 (1999); C. Bernard *et al.*, *ibid.* **61**, 111502 (2000).

[17] C. T. H. Davies *et al.* (HPQCD Collaboration), Phys. Rev. D **81**, 034506 (2010).

[18] G. P. Lepage *et al.* (HPQCD Collaboration), Nucl. Phys. B, Proc. Suppl. **106**, 12 (2002).

[19] C. Aubin *et al.* (MILC Collaboration), Phys. Rev. D **70**, 114501 (2004).

[20] C. T. H. Davies *et al.* (HPQCD Collaboration), Phys. Rev. D **78**, 114507 (2008).

[21] C. T. H. Davies *et al.* (HPQCD Collaboration), arXiv:1008.4018 [Phys. Rev. D (to be published)].

[22] C. Amsler *et al.*, Phys. Lett. B **667**, 1, 2008.

[23] A. Khodjamirian *et al.*, Phys. Rev. D **80**, 114005 (2009).

[24] Heavy Flavor Averaging Group, http://www.slac.stanford.edu/xorg/hfag/charm/index.html.

[25] D. Becirevic, S. Prelovsek, and J. Zupan, Phys. Rev. D **68**, 074003 (2003).

[26] C. Aubin and C. Bernard, Phys. Rev. D **76**, 014002 (2007).